PHYSICAL REVIEW C VOLUME 18, NUMBER 2 AUGUST 1978

Pre-equilibrium effects in fusion of ^{12}C and ^{158}Gd

D. G. Sarantites and L. Westerberg*
Department of Chemistry, Washington University, St. Louis, Missouri 63130

M. L. Halbert, R. A. Dayras, and D. C. Hensley
Oak Ridge National Laboratory, Oak Ridge, Tennessee 37830

J. H. Barker
Department of Physics, St. Louis University, St. Louis, Missouri 63103
(Received 4 May 1978)

Cross sections and the first three moments of the γ-ray multiplicity distribution were measured for many transitions in a series of $^{170-x}$Yb and $^{166-x}$Er products from bombardments of ^{158}Gd with ^{12}C at five energies corresponding to excitation in ^{170}Yb between 94 and 143 MeV. The average multiplicity for each xn channel increases with energy at first and then levels off at ~ 21. For the αxn channels saturation values between 16 and 20 are found. The excitation functions for $^{166-x}$Er indicate that the isotopes with small x are formed primarily by $2p(x+2)n$ evaporation and the ones with large x by αxn emission. A corresponding discontinuity in the average multiplicity vs x observed. These features are absent in ^{20}Ne + ^{150}Nd reactions at the same ^{170}Yb excitation, but are present in the ^{166}Er(^{4}He,xn) reactions at excitations from 63 to 92 MeV. The present results are clear indications of pre-equilibrium emission of neutrons and possibly of α particles, setting in at bombarding energies ~ 10 MeV per nucleon.

NUCLEAR REACTIONS ^{158}Gd(^{12}C,$xn\gamma$)$^{170-x}$Yb, $x=5$–11, ^{158}Gd(^{12}C, $\alpha xn\gamma$)$^{166-x}$Er, $x=4$–10, $E=112.0$, 124.7, 141.7, 152.7, 164.7 MeV, measured $\sigma(E)$, γ-ray average multiplicity, variance, and skewness; ^{158}Gd(^{12}C,$2\alpha xn\gamma$)$^{162-x}$Dy, $x=4$–7, $E=164.7$ MeV, measured σ; deduced angular momentum removal by γ rays and particles, J distributions in evaporation residues, pre-equilibrium effects. Enriched target.

I. INTRODUCTION

A large body of data on fusion of colliding heavy ions has been accumulated in recent years.[1,2] The results have been interpreted in terms of the formation and statistical decay of an equilibrated compound nucleus. Excitation functions[3-6] for a variety of reactions and energies (with $E \leq 10$ MeV/A) have been analyzed according to this model with some success. Measured charge or mass distributions for light systems such as ^{14}N + ^{12}C up to 248 MeV (Ref. 7) and ^{19}F + ^{27}Al up to 92 MeV (Ref. 8) have been well reproduced by statistical-model calculations. For the much heavier system ^{65}Cu + ^{86}Kr at 716 MeV evaporation residues are observed in the collisions with small impact parameter; the experimental distribution[9] is rather well reproduced by an evaporation calculation.[10] The possible importance of pre-equilibrium decay in heavy ion reactions has been discussed by Blann,[11] who calculated particle spectra and excitation functions for the ^{12}C + ^{141}Pr system at 100 and 200 MeV according to the hybrid model. He suggested that evidence for pre-equilibrium effects is found in the particle spectra of Galin *et al.*[12] from ^{14}N + ^{103}Rh at an excitation energy of 107 MeV. However, these may contain significant contributions from projectile fragmentation, deep-inelastic collisions, or other nonfusion processes, and therefore cannot be discussed in the context of pre-equilibrium evaporation from a fused system. In fact, recent work on reactions of 85- and 95-MeV ^{14}N on ^{209}Bi has shown that nearly all of the α-emission results from nonfusing collisions.[13] It has been suggested[14] that no persuasive experimental evidence yet exists that pre-equilibrium emission contributes significantly to deexcitation following fusion of heavy ions.

The experiments presented here and in the following paper[15] were designed to establish the extent to which pre-equilibrium emission of particles is present in heavy-ion induced reactions that lead to fusionlike products, its dependence on bombarding energy, entrance channel, and exit channel, and the role of angular momentum. This paper reports on reactions of ^{12}C + ^{158}Gd studied at five energies corresponding to excitations of 94.4, 106.2, 121.7, 132.0, and 143.1 MeV in the ^{170}Yb intermediate nucleus. The first four are approximately the same excitation energies at which ^{20}Ne + ^{150}Nd reactions were studied earlier.[16]

All possible coincidences between a Ge(Li) or a Ge(Li)-NaI anti-Compton spectrometer and nine NaI detectors were recorded. From these measurements the average multiplicity, the standard deviation, and the skewness of the multiplicity distribution as well as the production cross section for most of the Yb and Er reaction products were deduced.

The results from the present investigation indicate that pre-equilibrium effects set in at ~100 MeV of excitation in ^{170}Yb and become very important above ~130 MeV of excitation. This is in contrast with the ^{20}Ne + ^{150}Nd system where no evidence was found for pre-equilibrium emission at similar excitation energies.[16,17]

In the following paper[15] the results of two multiparameter coincidence experiments on ^{12}C + ^{158}Gd and ^{20}Ne + ^{150}Nd producing ^{170}Yb at about 132 MeV are presented. In those experiments coincidences between protons, α particles, or neutrons and γ rays characteristic of various products, together with the associated multiplicities, were recorded. Clear evidence for pre-equilibrium emission of both neutrons and α particles was obtained.

The point of view adopted in these two papers and in earlier ones[16,17] implicitly assumes that these Yb and Er products result from fusion of the projectile and target. It is difficult to visualize other processes that would lead to large yields of these products. We may consider, for example, (a) projectile fragmentation or (b) a deep-inelastic collision after which the reactants leave the scene of the interaction and the evaporation of light particles takes place later. (In the ^{20}Ne + ^{150}Nd system at 175.3 MeV, deep-inelastic and quasielastic processes account for roughly half the total reaction cross section.[18]) In either case, formation of Yb products by a deep-inelastic encounter would require that all the protons in the projectile transfer to the target and remain there. With the usual picture one does not expect such a strong preference for proton transfer in one direction only. Similarly, for the ^{20}Ne reactions leading to the Er products one would require that 8 of the 10 protons in the projectile end up in the targetlike fragment, which again seems rather unlikely in a deep-inelastic collision. These expectations are firmly supported by data from the ^{20}Ne + ^{150}Nd experiment of Ref. 18. The angle-integrated cross sections for the light fragments ($3 < Z < 10$) decrease rapidly with Z; the yields for $Z = 8$, 6, and 4 are in the ratio 50:20:1. For the ^{12}C reactions leading to Yb products the same argument applies. In the case of the Er products only four of the six protons need to be transferred to the target, and for the channels involving emission of relatively few particles, such as ^{158}Gd(^{12}C, $\alpha 4n$)^{162}Er, the argument against evaporation following nonfusing processes or projectile fragmentation becomes more difficult to support. However, these channels account for only a small part of the total cross section. Thus it seems reasonable to assume that fusion occurs in the great majority of the reactions studied here.

TABLE I. Bombardment conditions.

Beam	Thickness [a] (mg/cm^2)	Center-target beam (MeV)	^{170}Yb excitation energy (MeV)
$^{12}C^{4+}$	1.46	112.0	94.4
$^{12}C^{4+}$	1.46	124.7	106.2
$^{12}C^{5+}$	1.47	141.7	121.7
$^{12}C^{5+}$	1.46	152.7	132.0
$^{12}C^{5+}$	1.47	164.7	143.1

[a] Effective thickness to beam was 15–20% higher because of target tilt.

II. EXPERIMENTAL METHOD

The apparatus, method of measurement, and analysis of experiments to determine the first three moments of the distribution of the number of γ rays in cascade following heavy ion induced reactions have been discussed in detail elsewhere.[16,19] Only a brief description of the present experiment will be given here.

A. Beams

The ^{12}C beams were provided by the Oak Ridge Isochronous Cyclotron. Table I lists the bombardment conditions and the corresponding excitation energy in the ^{170}Yb intermediate nucleus. The cyclotron operated at frequencies between 8.89 and 10.61 MHz for these experiments, corresponding to a period between 94 and 112 ns. The length of the beam burst is typically a few percent of the period.

B. Targets

The targets were self-supporting, rolled foils of Gd metal, enriched to 92.0% in ^{158}Gd. Other isotopes of Gd were present in the percentages 0.96, 1.7, 3.56, and 1.82 for mass numbers 155, 156, 157, and 160, respectively. The thicknesses listed in Table I were determined by weighing the freshly rolled targets and measuring their areas. The 1.46-mg/cm^2 target was checked after bombardment by measuring the energy loss of 5.8-MeV α particles. The result was 1.43 mg/cm^2, in excellent agreement with the weight measurement. The targets were mounted on thin aluminum holders bent at 30° to the perpendicular to the beam and for some cases the target holder was rotated 15° to permit visibility to all detectors; this increased their effective thickness by 15 or 20%.

TABLE II. Experimental arrangements of the detectors. The angles are defined in a spherical polar coordinate system with its polar axis ($\theta = 0$) along the beam direction and its origin at the center of the target. The azimuthal angle ϕ is taken to be zero for the plane defined by the beam and the axis of the Ge(Li) detector.

Detector	Geometry A[a] θ (deg)	Geometry A[a] ϕ (deg)	Geometry B[b] θ (deg)	Geometry B[b] ϕ (deg)
Ge(Li)	90	0	90	0
NaI-1	140	0	45	270
NaI-2	50	0	135	270
NaI-3	45	180	45	180
NaI-4	90	180	90	180
NaI-5	135	180	135	180
NaI-6	69	139	69	139
NaI-7	111	139	111	139
NaI-8	69	221	69	221
NaI-9	111	221	111	221

[a] 112.0-, 124.7-, and 152.7-MeV runs.
[b] Anti-Compton arrangement, 141.7- and 164.7-MeV runs.

C. Ge(Li) counters

Two geometries were used in these experiments, geometry A of Table II for the 112.0-, 124.7-, and 152.7-MeV runs and geometry B, an anti-Compton arrangement, for the 141.7- and 164.7-MeV runs. In both cases the Ge(Li) detector was placed at 90° to the beam. For geometry A a 15% Ge(Li) was located 7 cm from the target. The resolution was 2.1 keV for the 243-keV $2^+ \to 0^+$ transition in ^{160}Yb. In geometry B, a 6.3% Ge(Li) detector was placed 14 cm from the target, inside a 14-cm-long by 19-cm-diam NaI annular detector surrounded by a 7.5-cm-thick Pb shield. The Ge(Li) was operated in anticoincidence with the annulus; an average suppression of the Compton background by a factor of 3.5 was acheived. The resolution was 1.5 keV at 243 keV.

The total Ge(Li) rate in the anti-Compton spectrometer was kept <3500/s, while the annular NaI detector was operating at $\leqslant$34 000/s. The total rate in each of the nine NaI detectors was <28 000/s. The timing resolution between the Ge(Li) and the annulus was ~60 ns (full width at tenth maximum). With a ^{60}Co source at the target position, the Compton-rejected spectrum did not show any full-energy peaks, indicating that the Pb shield and collimator effectively screened the annulus from a direct view of the target. For the multiplicity experiments without Compton suppression, the Ge(Li) rate was kept below 3500/s. The rate in each of the nine NaI detectors was $\leqslant$4500/s.

The Ge(Li) detectors were calibrated absolutely for the full-energy peak efficiency with γ sources of known strength placed at the target position. From this information, and from measurement of the integrated beam current and target thickness, the cross sections for the production of the various identified products were determined.

D. γ-ray multiplicity assembly

Nine 5.1-cm-diam by 7.6-cm-long NaI detectors were placed 10 cm from the target, each with its axis passing through the target center. Their angles are summarized in Table II for geometries A and B. In both cases a cast Pb shield housed seven of the NaI detectors, Nos. 3 to 9 of Table II; this apparatus is the "Urchin" of Ref. 19. The remaining two NaI detectors were surrounded by individual Pb shields to minimize crystal-to-crystal scattering. The Ge(Li)-NaI and NaI-NaI scattering was checked with ^{137}Cs and ^{54}Mn sources and found to be negligible.

Angular correlation corrections were applied for the geometries A and B. These were estimated for the 1-fold detection only [W_1 in Eq. (22) of Ref. 19] and were found to be 0.957 and 0.997, respectively. Corrections to higher-fold coincidence correlations were approximated as discussed in Refs. 16 and 19.

As in earlier experiments,[16,17] 0.5-mm Cd and 0.13-mm Cu absorbers were placed in front of each NaI detector. The lower-level discriminator thresholds were set to accept pulses $\geqslant$80 keV. The total efficiency of the NaI counters was then measured with standard sources of ^{109}Cd, ^{57}Co, ^{133}Ba, ^{137}Cs, and ^{60}Co at the target position. The average integral efficiency per NaI detector was found to be 0.0025, 0.0076, 0.0098, 0.0090, and 0.0081 at 88, 122, 340, 662, and 1275 keV, respectively. The efficiency at 2754 keV was found to be 0.0080 ± 0.0005 from multiplicity measurements with a ^{24}Na source.

Corrections for the response of the NaI detectors to neutrons were applied as discussed in Refs. 16 and 19. A constant efficiency of 0.0012 was used, which corresponds to 14% of their efficiency for 700-keV γ rays. The corrections lower the apparent multiplicities by about 12% and 3% for multiplicity values of 10 and 30, respectively.

E. Data accumulation

Coincidences between the Ge(Li) and the different NaI detectors within a 2τ resolving time of ~100 ns were recorded. For the 141.7- and 164.7-MeV ^{12}C runs the coincidence efficiency was 0.97 at 120 keV and unity above 200 keV. For the other runs it was 0.57, 0.62, 0.70, 0.78, 0.86, 0.92, and 0.98 at 120, 140, 180, 220,

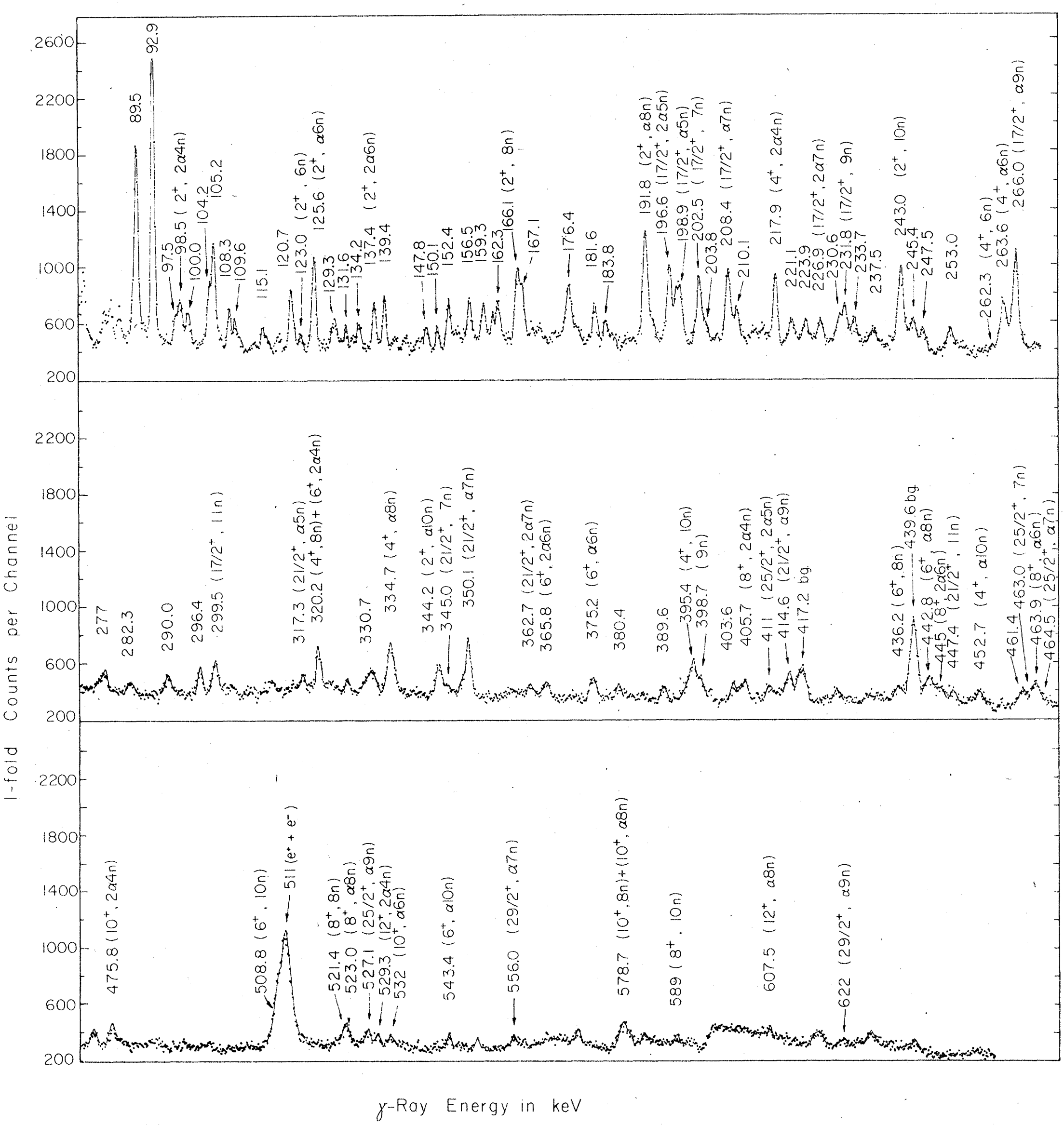

FIG. 1. Compton-suppressed spectrum recorded in 1-fold coincidence with nine NaI detectors from the 164.7-MeV ^{12}C bombardment of ^{158}Gd. The peaks from various exit channels are identified.

280, 350, and 500 keV, respectively, and unity above 800 keV.

The random coincidence rate was determined by means of a pulser triggered by the current integrator and was found to be $\leq 1.5\%$ for γ-ray multiplicities of ~20.

Nineteen 8192-channel Ge(Li) spectra were stored on disk by use of an on-line computer. Ten of these correspond to 0-fold up to 9-fold coincidences of all possible NaI combinations for each fold. The other nine were the separate 1-fold spectra.

III. RESULTS

A spectrum of the γ rays from the 164.7-MeV ^{12}C bombardment of ^{158}Gd recorded with the Ge(Li) detector under Compton suppression in 1-fold coincidence is shown in Fig. 1. As in other experiments of this type[16] at high bombardment energies the 0-fold spectra contain much background and many low-multiplicity lines. The peak-to-background ratio for the high-multiplicity exit channels is considerably better in the higher-fold spectra. The peak areas in each spectrum were extracted by means of a Gaussian peak-fitting program. Spectra corresponding to 0-, 1-, 2-, 3-, 4-, and the summed (5–9)-fold coincidences were analyzed for the γ rays from most of the exit channels. For the channels of highest multiplicity, the 0- to 5-fold and the summed (6–9)-fold spectra were analyzed.

A. Exit channels and gating transitions

For the two lowest ^{12}C bombardment energies, about 90–95% of the observed γ-ray line strength could be identified with transitions characteristic of known bands[20-27] in $^{160-165}$Yb and $^{156-162}$Er. Only a few weak transitions remain unidentified in these spectra. These may include lines from $^{169-x}$Tm (pxn) products, for which spectroscopic information is sparse. For the (^{12}C, 5n) reaction, the $\frac{19}{2}^+ \rightarrow \frac{15}{2}^+$ 338.8-keV transition was observed in addition to the ground state band. In all other cases except for ^{161}Yb only the ground state band was observed. At the highest bombardment energy the yield from the reaction (^{12}C, 2αxn)$^{162-x}$Dy was significant and additional yield went into unidentified lines.

Only one transition (232 keV) is known[5] in ^{161}Yb. The 9n cross sections reported in Ref. 16 are based on the yield of this line and appear to be low by a factor of ~2 compared to those for the 8n and 10n channels. In the present work, a previously[16] unresolved doublet was separated into a line at 395.3 keV, known[13] to be the $4^+ \rightarrow 2^+$ transition in ^{160}Yb, and a line at 398 keV. The latter has the same excitation function as the 232-keV line and so is most probably another transition in ^{161}Yb. In this work the 9n cross section was calculated from the sum of the yields of the 232- and 398-keV lines to make it fit smoothly between the 8n and 10n cross sections, suggesting that the two transitions occur in different bands. If so, the 9n cross sections of Ref. 16 should be increased by approximately a factor of 2. We have no spectroscopic information on the 398-keV transition; it has been arbitrarily labeled ($\frac{15}{2}^+ \rightarrow \frac{13}{2}^+$) in the tables and figures of this paper and the following paper.[15]

B. Cross sections

Absolute cross sections for many levels in each identified product were determined for the five ^{12}C bombardment energies. The cross sections were derived from the 90° yields in the Ge(Li) detector, multiplied by 1.15 to correct for angular distribution of stretched $E2$ cascades. Losses due to coincidence summing in the Ge(Li) detector were corrected as described in Ref. 19. Contributions due to isotopes in the target other than ^{158}Gd were subtracted, assuming that these reactions have the same excitation functions. These corrections were only a few percent for the prominent exit channels, but were as high as 20% for the channels with the lowest cross sections.

The resulting cross sections σ_J for individual transitions are listed in Table III and are plotted in Fig. 2 as a function of the spin J of the initial level. It is seen that σ_J decreases considerably with increasing J, indicating substantial population by side feeding. To obtain the total cross section for producing a particular product, the usual procedure[16,17] is to extrapolate the σ_J values to the ground state or the bandheads. With the present data this procedure could have led to large uncertainties at the highest bombarding energies for which only a few members of each band were observed. Consequently, the total cross section in this work were simply taken to be equal to the cross section for the lowest transition in each observed band. This is equivalent to the assumption that side feeding to the ground state is negligible. This seems reasonable for most of the even-A products [see Figs. 2(a), 2(c)–2(e)] although it may underestimate the cross sections for the odd-A products by about 15 or 20%.

The total cross sections are plotted in Fig. 3 as a function of incident energy. The cross sections σ_x for the (^{12}C,xn) reactions, plotted in Fig. 3(a), show considerable high-energy tailing a characteristic of pre-equilibrium emission.[11] The cross sections for the formation of ^{160}Er and ^{159}Er [Fig. 3(b)] exhibit two peaks which are displaced by an energy corresponding to 29 ± 3 MeV in excitation. This energy is very close to the binding energy of the α particle, suggesting that the higher peak corresponds to the process [^{12}C, 2$p(x+2)n$] while the lower one is due to (^{12}C, αxn). Further evidence for the occurrence of both the (^{12}C, αxn) and [^{12}C, 2$p(x+2)n$] reactions comes from measurement of the spectra of the particles emitted in coincidence with the γ rays characteristic of the Er isotopes.[15]

The sum of the cross sections for all the xn channels, plotted in Fig. 3(a), decreases by a factor of 2 as the bombardment energy increases from 112.0 to 164.7 MeV. In contrast, the total cross section for the formation of all Er products [Fig. 3(b)] increases by a factor of 2 over the same energy range.

C. Average multiplicities

The average multiplicity $\langle M_{\text{in}}^i \rangle$ of the incoming cascades to a level i that de-excites by the gating transition was calculated using the computer program[19] GETM. In this case the incoming

TABLE III. Cross sections for individual γ transitions in reaction products from bombardments of ^{158}Gd with ^{12}C. The underlined numbers are estimates of the statistical error and refer to the least significant figures given.

Product	E_γ (keV)	Transition $J_i^\pi \to J_f^\pi$	σ_J (mb) E_{lab} (MeV) 112.0	124.7	141.7	152.7	164.7
^{165}Yb + 5n	206.1	$\frac{17}{2}^+ \to \frac{13}{2}^+$		15 2			
	429.2	$\frac{25}{2}^+ \to \frac{21}{2}^+$	38 6	21 5			
	523.5	$\frac{29}{2}^+ \to \frac{25}{2}^+$	23 8				
	338.8	$\frac{19}{2}^+ \to \frac{15}{2}^+$	23 3	16 3			
$\sigma(^{165}$Yb)			38 6	16 4			
^{164}Yb + 6n	123.3	$2^+ \to 0^+$	158 24	45 7	16 5		19 3
	262.3	$4^+ \to 2^+$	159 6	38 9			
	374.7	$6^+ \to 4^+$	158 15	19 4			
	463.2	$8^+ \to 6^+$	110 20 [a]				
	530.5	$10^+ \to 8^+$	77 7	19 5			
	576.5	$12^+ \to 10^+$	67 7				
	490.0	$16^+ \to 14^+$	48 5				
	543.2	$18^+ \to 16^+$	29 5				
	632.5	$20^+ \to 18^+$	39 6				
$\sigma(^{164}$Yb)			158 10	45 6			
^{163}Yb + 7n	202.8	$\frac{17}{2}^+ \to \frac{13}{2}^+$	415 5	206 5	73 2	31 4	
	345.0	$\frac{21}{2}^+ \to \frac{17}{2}^+$	294 6	133 4	21 2	21 5	55 3
	463.0	$\frac{25}{2}^+ \to \frac{21}{2}^+$	180 21 [a]				
	557.3	$\frac{29}{2}^+ \to \frac{25}{2}^+$	128 16	73 8			
	629.9	$\frac{33}{2}^+ \to \frac{29}{2}^+$	101 6				
$\sigma(^{163}$Yb)			415 20	206 10	73 5	33 10	55 15
^{162}Yb + 8n	166.3	$2^+ \to 0^+$	289 8	507 6	192 3	147 7	80 2
	320.3	$4^+ \to 2^+$	255 5	486 6	185 2	112 7	63 2
	436.7	$6^+ \to 4^+$	161 8	295 8	139 2	74 4	20 4
	521.4	$8^+ \to 6^+$	91 8	177 11		(50 25)	
	610.5	$12^+ \to 10^+$	55 6				
$\sigma(^{162}$Yb)			282 20	507 30	192 15	147 15	80 10
^{161}Yb + 9n	232	$\frac{17}{2}^+ \to \frac{13}{2}^+$		50 4	127 2	119 3	44 2
	398	$(\frac{15}{2}^+ \to \frac{13}{2}^+)$		41 5	110 3	98 20	66 10
$\sigma(^{161}$Yb)				91 10	237 30	217 30	110 20
^{160}Yb + 10n	243.0	$2^+ \to 0^+$			43 1	145 5	132 10
	395.3	$4^+ \to 2^+$			62 3	125 6	157 15
	508.8	$6^+ \to 4^+$			(107 4) [b]	(199 8) [b]	(232 5) [b]
$\sigma(^{160}$Yb)					43 5	145 15	135 10
^{159}Yb + 11n	299.5	$\frac{17}{2}^+ \to \frac{13}{2}^+$				24 3	52 2
	549.3	$\frac{25}{2}^+ \to \frac{21}{2}^+$					12 2
$\sigma(^{159}$Yb)						24 3	52 6

TABLE III. (*Continued*).

Product	E_γ (keV)	Transition $J_i^\pi \rightarrow J_f^\pi$	σ_J(mb) E_{lab} (MeV) 112.0	124.7	141.7	152.7	164.7
^{162}Er + ($4n\alpha + 2p6n$)	227.5	$4^+ \rightarrow 2^+$	33 4	33 3	26 1		
	337.1	$6^+ \rightarrow 4^+$	32 5		19 1		
$\sigma(^{162}$Er)			33 4	33 3	22 2		
^{161}Er + ($5n\alpha + 2p7n$)	198.6	$\frac{17}{2}^+ \rightarrow \frac{13}{2}^+$			57 3		
	318.5	$\frac{21}{2}^+ \rightarrow \frac{17}{2}^+$	82 4	55 4	20 2	32 5	13 2
	425.1	$\frac{25}{2}^+ \rightarrow \frac{21}{2}^+$	51 5	29 3		30 4	21 2
	518.5	$\frac{29}{2}^+ \rightarrow \frac{25}{2}^+$	35 6	25 6			
$\sigma(^{161}$Er)			118 20	77 15	57 3	33 5	17 2
^{160}Er + ($6n\alpha + 2p8n$)	125.6	$2^+ \rightarrow 0^+$	160 6	171 7	119 3	192 9	145 3
	263.9	$4^+ \rightarrow 2^+$	118 5	127 11	59 2	98 3	82 2
	375.5	$6^+ \rightarrow 4^+$	60 14	99 4	65 2	53 4	47 2
	531.7	$10^+ \rightarrow 8^+$	(130 6)	83 5			
	591.9	$14^+ \rightarrow 12^+$	46 6				
	534.0	$16^+ \rightarrow 14^+$	38 6				
	555.4	$18^+ \rightarrow 16^+$	41 16				
$\sigma(^{160}$Er)			160 20	160 20	110 15	192 20	145 20
^{159}Er + ($7n\alpha + 2p9n$)	208.5	$\frac{17}{2}^+ \rightarrow \frac{13}{2}^+$	30 4	82 4	70 2	87 4	67 2
	349.9	$\frac{21}{2}^+ \rightarrow \frac{17}{2}^+$	10 4	48 3	99 2	58 5	120 4
	464.5	$\frac{25}{2}^+ \rightarrow \frac{21}{2}^+$	28 7				
	556.0	$\frac{29}{2}^+ \rightarrow \frac{25}{2}^+$			65 3		
	626.0	$\frac{33}{2}^+ \rightarrow \frac{29}{2}^+$			34 2		56 4
$\sigma(^{159}$Er)			30 4	82 10	90 20	87 10	92 20
^{158}Er + ($8n\alpha + 2p10n$)	192.7	$2^+ \rightarrow 0^+$		44 4	120 2	180 5	153 2
	335.6	$4^+ \rightarrow 2^+$		29 3	86 2	119 4	114 3
	443.8	$6^+ \rightarrow 4^+$		44 5	82 2	78 4	37 4
	523.8	$8^+ \rightarrow 6^+$				100 26	73 3
	608.1	$12^+ \rightarrow 10^+$					43 7
$\sigma(^{158}$Er)				36 3	110 15	140 20	140 20
^{157}Er + $9n\alpha$	266.4	$\frac{17}{2}^+ \rightarrow \frac{13}{2}^+$			28 1	115 3	136 2
	414.8	$\frac{21}{2}^+ \rightarrow \frac{17}{2}^+$			26 2	67 5	59 5
	572.2	$\frac{25}{2}^+ \rightarrow \frac{21}{2}^+$					37 3
$\sigma(^{157}$Er)					28 5	115 15	135 15
^{156}Er + $10n\alpha$	453.0	$4^+ \rightarrow 2^+$			16 2	38 8	49 4
	544.0	$6^+ \rightarrow 4^+$					21 2
	674.0	$10^+ \rightarrow 8^+$					29 4
$\sigma(^{156}$Er)					16 3	38 8	49 10
^{158}Dy + $4n2\alpha$	98.8	$2^+ \rightarrow 0^+$					159 8
	218.2	$4^+ \rightarrow 2^+$					75 2
	406.3	$8^+ \rightarrow 6^+$					46 2

TABLE III. (*Continued*).

Product	E_γ (keV)	Transition $J_i^\pi \to J_f^\pi$	σ_J(mb) E_{lab} (MeV) 112.0	124.7	141.7	152.7	164.7
	476.0	$10^+ \to 8^+$					42 $\underline{3}$
$\sigma(^{158}Dy)$							90 $\underline{20}$
$^{157}Dy + 5n2\alpha$	196.9	$\frac{17}{2}^+ \to \frac{13}{2}^+$					100 $\underline{2}$
$\sigma(^{157}Dy)$							100 $\underline{20}$
$^{156}Dy + 6n2\alpha$	137.7	$2^+ \to 0^+$					53 $\underline{2}$
	366.4	$6^+ \to 4^+$					34 $\underline{2}$
$\sigma(^{156}Dy)$							50 $\underline{10}$
$^{155}Dy + 7n2\alpha$	227.4	$\frac{17}{2}^+ \to \frac{13}{2}^+$					32 $\underline{2}$
	363.2	$\frac{21}{2}^+ \to \frac{17}{2}^+$					15 $\underline{2}$
$\sigma(^{155}Dy)$							25 $\underline{5}$

[a] Resolved into 463.2, 463.0, and 463.9 keV from the $6n$, $7n$, and $6n\alpha$ products on the basis of J dependence of σ_J for nearby J values.

[b] Difficult to resolve from strong nearby peak.

cascades to a level include both the cascades via (observed) higher-lying levels in the same band and the side feeding cascades entering the level from other (unobserved) bands. The average multiplicity $\langle M_J \rangle$ for a level i with spin J was then calculated as the sum $\langle M_J \rangle = \langle M_{in}^{(i)} \rangle + M_{out}^{(i)}$, where $M_{out}^{(i)}$ is the known number of transitions from the ith level to the ground state. The individual values for $\langle M_J \rangle$ are available in Ref. 28.

Most of the $\langle M_J \rangle$ values for the 112.0-, 124.7-,

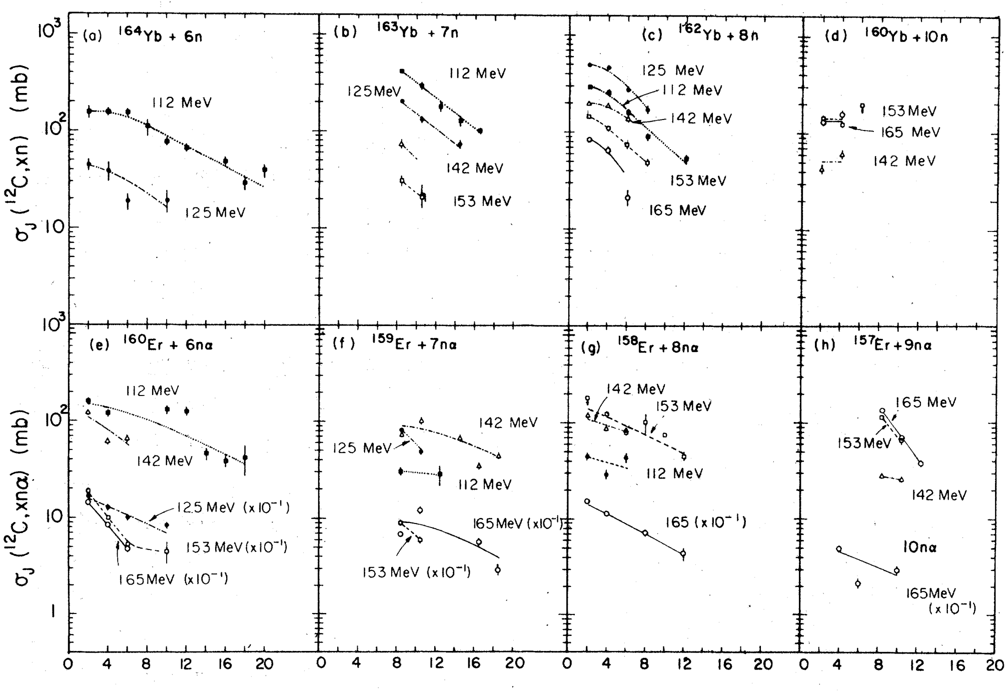

FIG. 2. Measured cross sections σ_J from bombardments of ^{158}Gd with ^{12}C at the indicated energies for levels observed in the various identified reaction products, as a function of $J_{initial}$ of the gating transition. The smooth lines are to guide the eye.

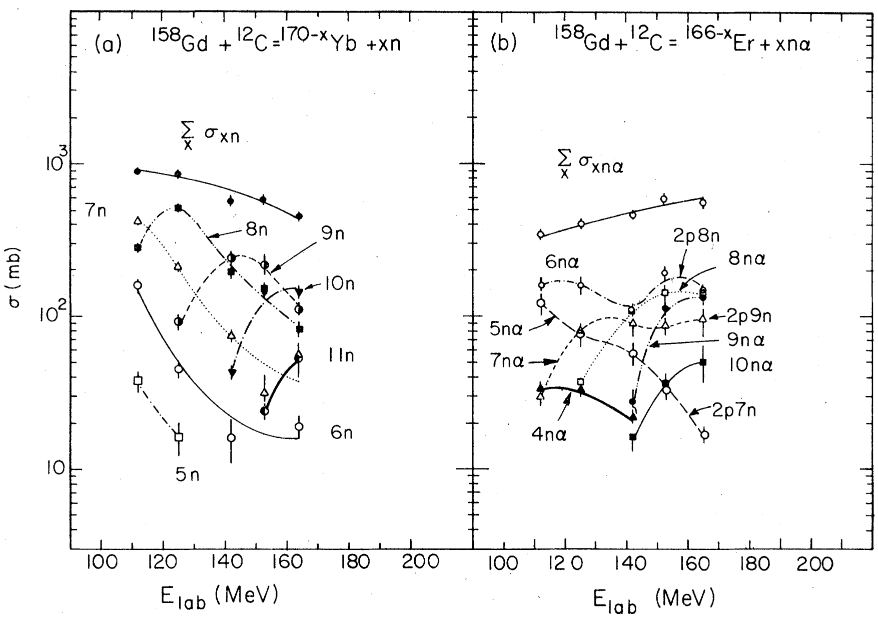

FIG. 3. Excitation functions of the products formed in the bombardments of ^{158}Gd with ^{12}C. The cross sections correspond to transitions to the ground state or to the band head for the odd A cases. The sums of all the xn or $xn\alpha$ channels are also shown.

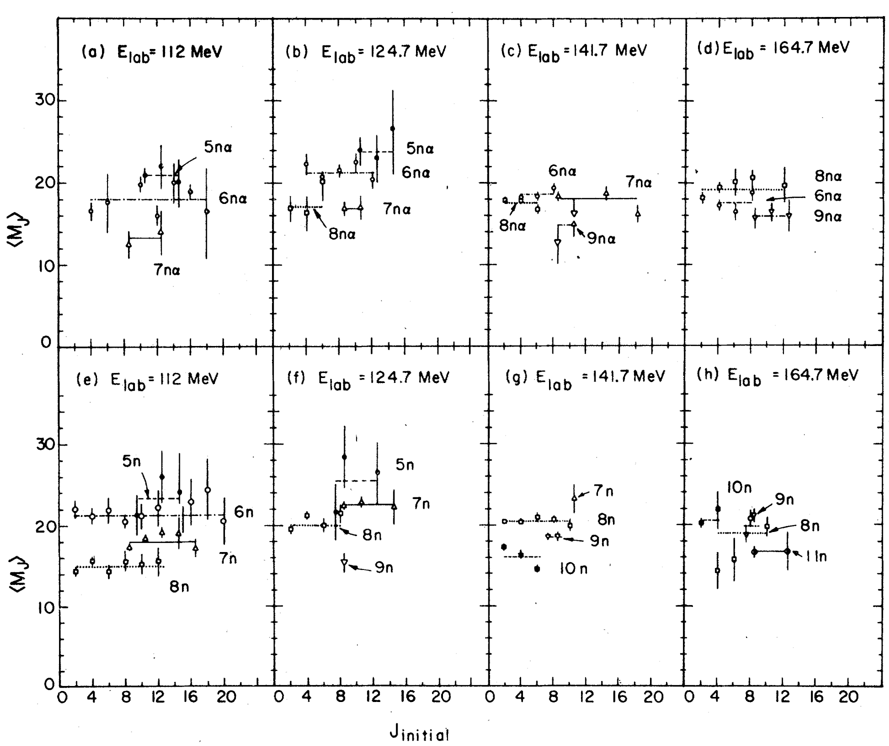

FIG. 4. Average multiplicity $\langle M_J \rangle$ as a function of J_{initial} for the gating transition in the various reaction products formed in the bombardments of ^{158}Gd by ^{12}C at 112.0, 124.7, 141.7, and 164.7 MeV. The lines are to guide the eye. The $\langle M_J \rangle$ values are seen to be independent of J_{initial}.

TABLE IV. Summary of the total multiplicity $\langle M\rangle_x$, width σ_{M_x}, and skewness s_{M_x} of the γ cascades in the various identified evaporation residues following bombardments of ^{158}Gd with ^{12}C at the indicated laboratory energies.

Reaction product	E_{lab} = 112.0 MeV $\langle M\rangle_x$	σ_{M_x}	E_{lab} = 124.7 MeV $\langle M\rangle_x$	σ_{M_x}	E_{lab} = 141.7 MeV $\langle M\rangle_x$	σ_{M_x}	s_{M_x}	E_{lab} = 152.7 MeV $\langle M\rangle_x$	σ_{M_x}	s_{M_x}	E_{lab} = 164.7 MeV $\langle M\rangle_x$	σ_{M_x}	s_{M_x}
^{165}Yb + 5n	23.3 $\underline{18}$	5 $\underline{17}$	25.6 $\underline{20}$										
^{164}Yb + 6n	21.3 $\underline{5}$	6.0 $\underline{18}$	24.0 $\underline{23}$	9.5 $\underline{35}$									
^{163}Yb + 7n	17.0 $\underline{2}$	3.9 $\underline{11}$	22.6 $\underline{5}$	3.2 $\underline{38}$	21.5 $\underline{16}$	10.5 $\underline{10}$	−0.5 $\underline{6}$	20.3 $\underline{33}$	6 $\underline{7}$	−0.2 $\underline{8}$	20.2 $\underline{10}$	7.7 $\underline{29}$	
^{162}Yb + 8n	14.2 $\underline{2}$	5.9 $\underline{8}$	20.12 $\underline{16}$	4.0 $\underline{13}$	29.49 $\underline{13}$	10.6 $\underline{6}$	−1.5 $\underline{6}$	20.9 $\underline{8}$	10 $\underline{2}$		19.0 $\underline{12}$	9.5 $\underline{10}$	−0.8 $\underline{9}$
^{161}Yb + 9n			15.3 $\underline{12}$		18.5 $\underline{2}$	9.1 $\underline{10}$	−1.3 $\underline{10}$	20.9 $\underline{7}$	7.5 $\underline{26}$		19.8 $\underline{7}$	9.7 $\underline{19}$	−1.7 $\underline{23}$
^{160}Yb + 10n					15.0 $\underline{3}$	8.6 $\underline{10}$	−0.8 $\underline{10}$	19.0 $\underline{4}$	8.0 $\underline{11}$	−1.5 $\underline{14}$	20.4 $\underline{3}$	9.5 $\underline{8}$	−0.7 $\underline{4}$
^{159}Yb + 11n								17.3 $\underline{19}$			16.7 $\underline{7}$	8.2 $\underline{18}$	
^{162}Er + α4n	18.7 $\underline{15}$	8.8 $\underline{40}$			22.5 $\underline{15}$	9.6 $\underline{30}$	0.0 $\underline{13}$						
^{161}Er + α5n	20.9 $\underline{9}$	5.9 $\underline{32}$	23.7 $\underline{14}$	7.6 $\underline{81}$	17.7 $\underline{16}$	9.2 $\underline{16}$	0.0 $\underline{12}$	21.7 $\underline{23}$	9 $\underline{6}$		22.5 $\underline{16}$	7.4 $\underline{50}$	
^{160}Er + α6n	18.3 $\underline{5}$	6.5 $\underline{12}$	21.2 $\underline{4}$	5.5 $\underline{20}$	18.6 $\underline{3}$	10.3 $\underline{8}$	−0.4 $\underline{6}$	18.9 $\underline{7}$	8.1 $\underline{19}$		17.6 $\underline{4}$	9.4 $\underline{8}$	−0.4 $\underline{9}$
^{159}Er + α7n	13.3 $\underline{14}$	6.7 $\underline{33}$	16.8 $\underline{8}$		18.1 $\underline{4}$	10.1 $\underline{10}$	−0.35 $\underline{60}$	16.9 $\underline{7}$	6.0 $\underline{27}$		16.7 $\underline{4}$	10.0 $\underline{5}$	0.3 $\underline{3}$
^{158}Er + α8n			17.0 $\underline{12}$	8.7 $\underline{33}$	17.6 $\underline{2}$	9.8 $\underline{10}$	−1.0 $\underline{8}$	18.4 $\underline{4}$	9.0 $\underline{12}$	−0.8 $\underline{12}$	19.1 $\underline{3}$	10.5 $\underline{6}$	−1.2 $\underline{5}$
^{157}Er + α9n					15.7 $\underline{18}$	8.8 $\underline{30}$		16.2 $\underline{10}$	5.8 $\underline{17}$		16.0 $\underline{8}$	9.5 $\underline{6}$	−0.7 $\underline{5}$
^{156}Er + α10n								16.3 $\underline{22}$	9.6 $\underline{47}$		18.7 $\underline{10}$	8.9 $\underline{25}$	
^{158}Dy + 2α4n											10.5 $\underline{3}$	8.2 $\underline{5}$	0.5 $\underline{5}$
^{157}Dy + 2α5n											8.9 $\underline{3}$	9.3 $\underline{5}$	0.9 $\underline{4}$
^{156}Dy + 2α6n											11.2 $\underline{4}$	8.6 $\underline{8}$	0.5 $\underline{7}$
^{155}Dy + 2α7n											11.1 $\underline{8}$	7.9 $\underline{18}$	

141.7-, and 164.7-MeV bombardments are shown in Figs. 4(a)–4(h). It appears that $\langle M_J\rangle$ is the same for all levels in a given product. In view of this fact the $\langle M_J\rangle$ values for all levels in each product were combined to obtain the average multiplicity designated by $\langle M\rangle_x$ for a channel corresponding to emission of x neutrons. These results are summarized in Table IV.

The values of $\langle M\rangle_x$ for the (^{12}C,xn) $^{170-x}$Yb and (^{12}C, αxn) $^{166-x}$Er reactions are plotted in Figs. 5(a) and 5(b) as a function of the excitation energy of the intermediate nucleus ^{170}Yb. The multiplicity of the xn channels is seen in Fig. 5(a) to increase at first, then level off and decrease somewhat with increasing excitation energy. This is to be contrasted with the behavior of $\langle M\rangle_x$ from the ^{150}Nd(^{20}Ne,xn) reactions[16,17] leading to the same intermediate nucleus ^{170}Yb at nearly the same excitation energies, as shown in Fig. 5(a). Very similar behavior is observed in Fig. 5(b) for the αxn products. Here it should be pointed out that Fig. 5(b) shows only the $\langle M\rangle_x$ believed to be associated with the (^{12}C, αxn) and not the [^{12}C, $2p(x+2)n$] channels, according to the demarcation suggested by Fig. 3(b).

The cross sections and multiplicities for each exit channel can be displayed in another instructive way by plotting the total cross sections and average multiplicities from the (^{12}C,xn) reactions vs x, the number of emitted neutrons. In Fig. 6 the open circles give σ_x and $\langle M\rangle_x$ for the five excitation energies investigated, while the full squares give these quantities for the (^{20}Ne,xn) reactions interpolated from the data of Refs. 16 and 17 for the same excitation energies. For the lowest two energies the cross sections from both reactions are essentially symmetric about the most probable x, but in going to higher excitations a tail develops for the (^{12}C,xn) cross sections for low x, which of course results from the tailing in the excitation functions shown in Fig. 3.

The multiplicities $\langle M\rangle_x$ from (^{12}C,xn) are compared with those from the (^{20}Ne,xn) reactions in Figs. 6(f)–6(i). For ^{20}Ne, $\langle M\rangle_x$ increases with decreasing x. This is the behavior expected in statistical decay of a compound nucleus, for if the x neutrons are evaporated with energies governed by the statistical model, then evaporation of fewer neutrons will leave more energy for γ-ray emission. For ^{12}C, however, the $\langle M\rangle_x$ values deviate from this trend more and more strongly as the excitation increases. At the highest energies $\langle M\rangle_x$ remains essentially constant for small x. That is, as fewer neutrons are emitted, the number of γ rays does not increase, implying that one or more of the neutrons must carry off

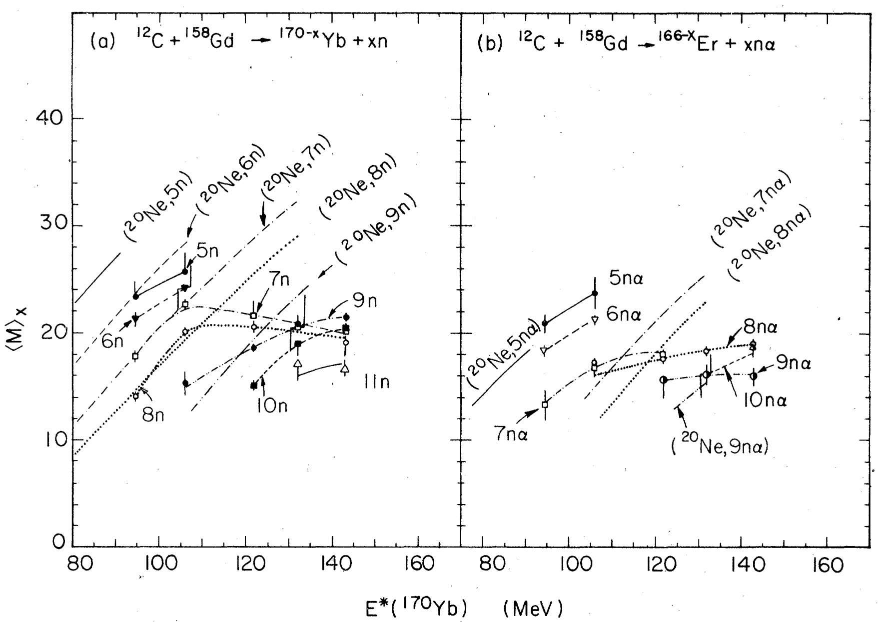

FIG. 5. Average multiplicity $\langle M \rangle_x$ of the γ cascades that populate the ground state of the various products formed in the reactions indicated as a function of excitation energy in ^{170}Yb. The lines through the data points are to guide the eye. The lines marked (^{20}Ne,xn) and (^{20}Ne,$xn\alpha$) are from Ref. 16 for comparison.

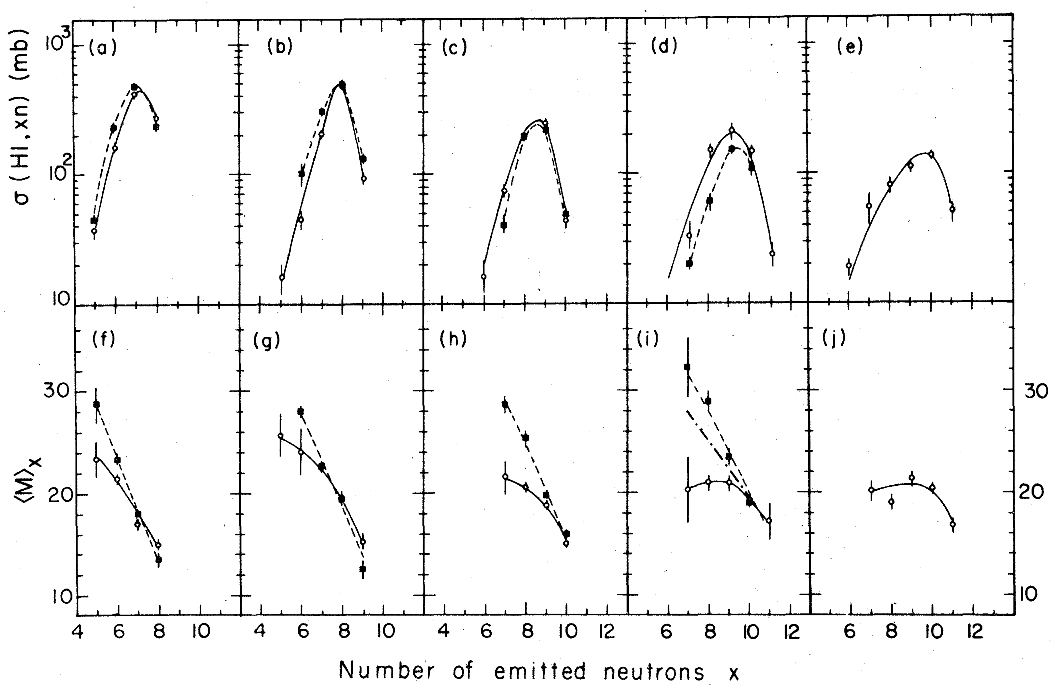

FIG. 6. Total cross sections σ_x and multiplicities $\langle M \rangle_x$ for the various xn products formed in the reactions of ^{12}C + ^{158}Gd (open circles, solid lines) and ^{20}Ne + ^{150}Nd (full squares, dashed lines) at the indicated excitation energies as a function of the number of emitted neutrons. The ^{170}Yb excitation energies in MeV are 94.4 (a,f), 106.2 (b,g), 121.7 (c,h), 132.0 (d,i), and 143.1 (e,j). The lines through the data are to guide the eye. Note the shift of the left wing of the (^{12}C, xn) cross sections as the energy increases and the leveling off of $\langle M \rangle_x$ at the higher excitations.

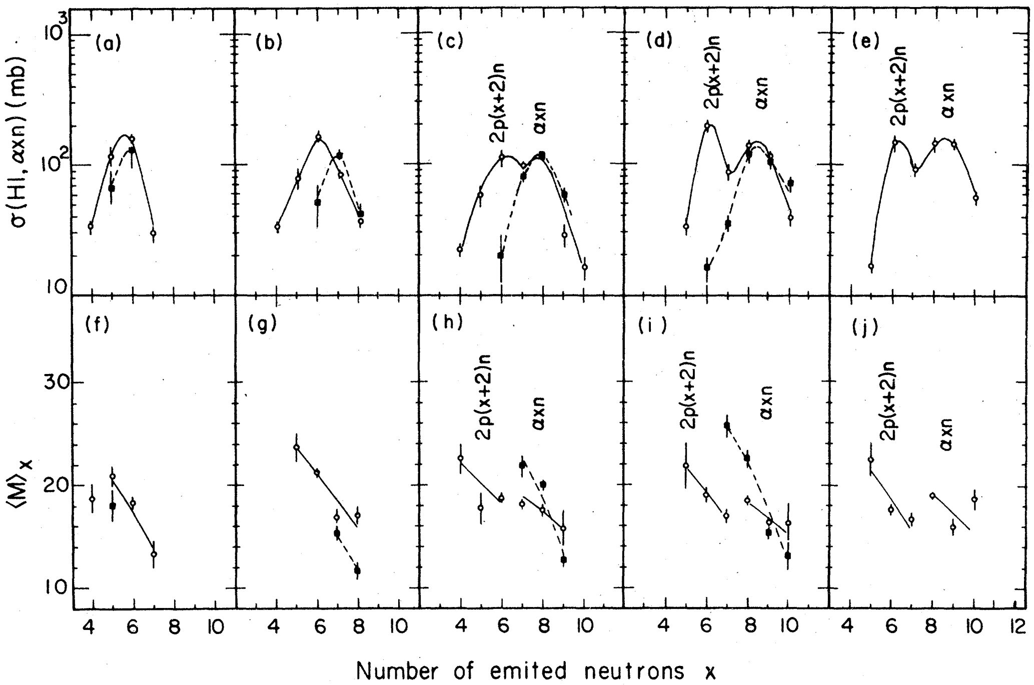

FIG. 7. Total cross section σ_x and multiplicities $\langle M\rangle_x$ for the formation of $^{166-x}$Er isotopes from reactions of ^{12}C + ^{158}Gd (open circles) and ^{20}Ne + ^{150}Nd (full squares) as a function of the number of emitted neutrons. The excitation energies are the same as in Fig. 6. The lines through the data are to guide the eye.

a great deal of energy. This behavior is similar to that observed[17] for (^{4}He,xn) reactions in which it has been established[11] that pre-equilibrium emission of neutrons is important.

Similar plots are given in Fig. 7 for the ^{12}C and ^{20}Ne reactions leading to $^{166-x}$Er products. The open circles in Fig. 7 again denote quantities from the ^{12}C reactions and the full squares are interpolated from the data of Refs. 16 and 17 for the ^{20}Ne reactions for the same excitation energies. As the excitation energy is increased, a double peak appears in the yield of the Er isotopes produced by ^{12}C beams. A comparison of this result with the excitation functions of Fig. 3(b) clearly indicates that the peak at lower x is associated with the [^{12}C, $2p(x+2)n$] reactions. This dual mode for the production of $^{166-x}$Er in ^{12}C induced reactions is further substantiated by the multiplicities shown in Figs. 7(f)–7(j). For excitation energies above 121.7 MeV, there seems to be a discontinuity in $\langle M\rangle_x$ just at the valley in the cross sections. The multiplicities for the [^{12}C, $2p(x+2)n$] channels shown in the small-x parts of Figs. 7(h)–7(j) are in excellent agreement with the results in Figs. 6(h)–6(j) for the (^{12}C,xn) channels that involve the same number of emitted nucleons. The behavior of $\langle M\rangle_{\alpha xn}$ for small x is obscured in these experiments by the $2p(x+2)n$ channels. In the experiments of Ref. 15, where the emitted α particles are detected in coincidence with the γ rays characteristic of $^{166-x}$Er, this region has been successfully explored.

D. Higher moments

The standard deviation σ_{M_J} of the multiplicity distribution for the cascades via a state with spin J was taken to be the same as the width of the distribution of the incoming cascades, since for all identified products no branching occurs for the part of the γ cascade below the gating transition. The individual values of σ_{M_J} may be found in Ref. 28. Within experimental error the widths σ_{M_J} are independent of J. The average widths σ_{M_J} for each exit channel are summarized in Table IV and are plotted vs x and incident energy in Fig. 8.

For the $7n$ and $8n$ channels, the widths appear first to increase, and then level off when the bombardment energy is increased. The turning point seems to coincide with the energy where deviations from the statistical evaporation are observed [see Figs. 6(h)–6(j)].

Meaningful values for the skewness, averaged over J of the initial state, s_{M_x}, were obtained for most of the exit channels seen in the 141.7- and 164.7-MeV runs that employed the anti-Compton spectrometer, but for only a few of the other

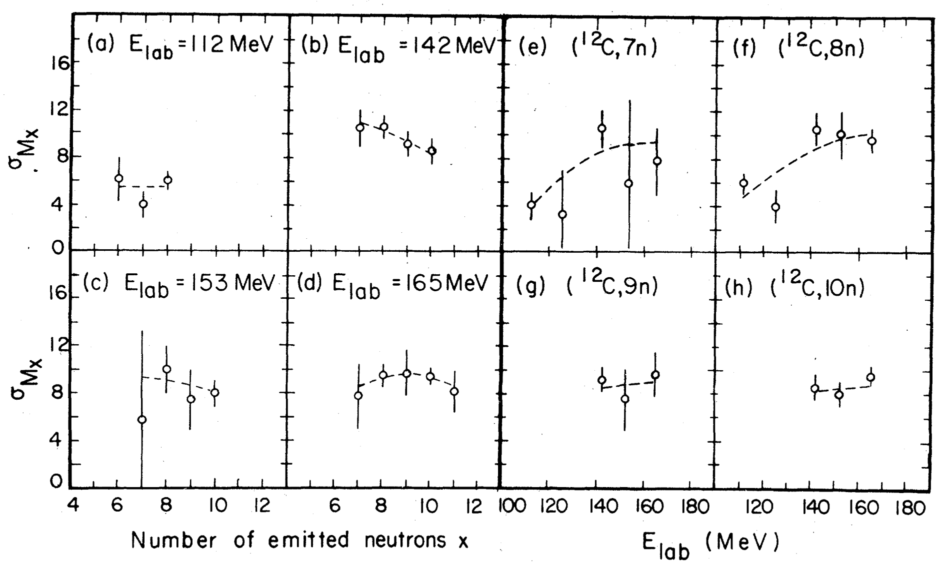

FIG. 8. Widths σ_{M_x} of the multiplicity distributions from $^{12}C + ^{158}Gd$ as a function of the number of emitted neutrons x at the indicated bombardment energies (a)–(d) and as a function of bombardment energy for the various xn channels (e)–(h).

bombardments. The results are summarized in Table IV. Values of skewness for various gating transitions are given in Ref. 28.

IV. RELATION OF MULTIPLICITY TO ANGULAR MOMENTUM

A. Total multiplicity and total angular momentum distributions

Valuable information about the reaction mechanism can be obtained by relating the moments of the γ-ray multiplicity distribution to the corresponding moments of the angular momentum distribution in the "entry states," i.e., the states prior to γ decay. In the following, the total γ-ray multiplicities $\langle M\rangle_{\overline{xn}}$ and $\langle M\rangle_{\overline{\alpha xn}}$ at given bombardment energy are defined as the weighted average over all xn and αxn channels, respectively, by the expressions

$$\langle M\rangle_{\overline{xn}} = \frac{\sum_x \sigma_{xn}[\langle M\rangle_{xn} + \frac{1}{2}J_g]}{\sum_x \sigma_{xn}} \tag{1a}$$

and

$$\langle M\rangle_{\overline{\alpha xn}} = \frac{\sum_x \sigma_{\alpha xn}[\langle M\rangle_{\alpha xn} + \frac{1}{2}J_g]}{\sum_x \sigma_{\alpha xn}}\,, \tag{1b}$$

where J_g is the angular momentum of the state where the cascade terminates. As in earlier work,[16,17,29] we relate the average angular momentum $\langle J\rangle_{\overline{xn}}$ of the xn entry states to the average angular momentum $\langle l_{ER}\rangle$ of the initial states before particle evaporation by

$$\langle l_{ER}\rangle = \langle J\rangle_{\overline{xn}} + f_n\langle x\rangle\,, \tag{2}$$

where f_n is the angular momentum carried off on the average by each of the x neutrons.

Estimates of $\langle l_{ER}\rangle$ may be made from the sharp-cutoff model (triangular distribution of initial states) if the total evaporation cross section σ_{ER}

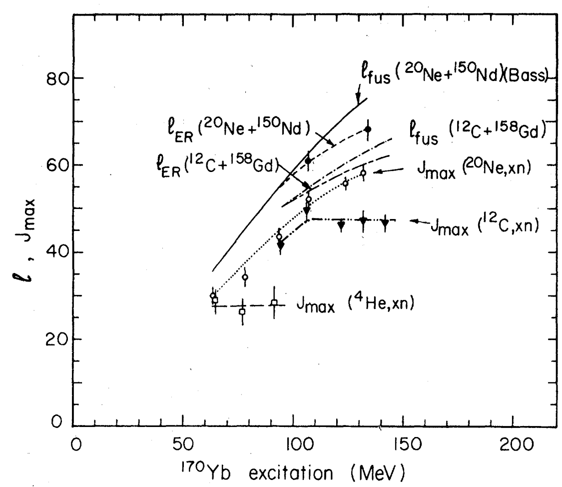

FIG. 9. Variation of maximum angular momenta for $^{170-x}$Yb products prior to γ decay as a function of excitation energy. The solid line gives the predictions of the Bass model (Ref. 30) of l_{fus} for the reactions of $^{20}Ne + ^{150}Nd$. The dashed line and the full circles give the l_{ER} values based on σ_{ER} measurements (Refs. 18 and 31). The open circles are the J_{max} values from the multiplicity measurements for the (^{20}Ne, xn) reactions (Refs. 16 and 17). The dash-dot line is l_{ER} for the $^{12}C + ^{158}Gd$ system from the Bass model after correction for fission. The full triangles give the J_{max} values from the multiplicity measurements in the (^{12}C,xn) products. The open squares are from Ref. 17 for $^4He + ^{166}Er$ reactions.

TABLE V. Cross sections and angular momenta characterizing the ^{20}Ne + ^{150}Nd reactions. The experimental data are from Refs. 16 and 17 except as noted.

	E_{lab} (MeV) 94.2	110.7	128.0	144.0	163.5	172.4
E^*(^{170}Yb, MeV)	63.2	77.7	93.7	107.0	124.3	132.1
E_{lab}/A (MeV)	4.71	5.54	6.40	7.20	8.18	8.62
σ_{fus} (mb) [a]	570	830	1040	1200	1335	1385
σ_{ER} (mb) [b]	570	830	1010	1111 [c]	1135	1150 ± 90 [d]
l_{crit}	35.2	46.2	55.7	63.5	71.4	74.7
l_{ER}	35.2	46.2	54.9	61.1	65.8	68.1
$\langle M\rangle_{\overline{xn}}$	14.8 8	16.0 8	19.4 5	22.5 7	24.0 5	25.0 6
$\langle x\rangle$	5.09	5.96	6.9	7.5	8.6	9.0
$\langle M\rangle_{\overline{\alpha xn}}$		17.45 80	18.7 15	18.0 12	20.35 50	19.75 40
$\langle x\rangle_\alpha$		4.8	5.7	7.0	8.2	8.6
$\langle M_s\rangle$	4.3	4.6	4.8	5.1	5.5	5.6
f_s (adopted)	0.32	0.35	0.37	0.39	0.42	0.43
f_n (deduced)	0.40	0.40	0.38	0.40	0.40	0.40
$\langle J\rangle_{\overline{xn}}$	22.4 16	24.4 16	31.0 10	36.8 14	39.3 10	41.2 12
$\langle J\rangle_{\overline{\alpha xn}}$		27.3 16	29.6 30	27.8 24	32.0 10	30.5 8
f_α		1.6 16	4.8 30	10.1 24	8.6 10	11.5 8

[a] Prediction from the Bass model, Ref. 30.
[b] Except as noted, from σ_{fus} with an empirical estimate of fission subtracted, the latter from Ref. 31.
[c] Reference 31.
[d] Reference 18.

is known. The present measurements of xn and αxn cross sections do not constitute a measurement of the evaporation cross section because of the unidentified (HI,pxn) channels, so we must consider some theoretical prediction. For ^{20}Ne + ^{150}Nd reactions up to 175 MeV (excitation up to 134 MeV in ^{170}Yb), Halbert *et al.*[18] have shown that predictions of the fusion cross section by the Bass model[30] are consistent with experiment. Therefore we have used this model to predict the

TABLE VI. Cross sections and angular momenta characterizing the ^{12}C + ^{158}Gd reactions.

	E_{lab} (MeV) 112.0	125.0	141.7	152.0	164.7
E^*(^{170}Yb, MeV)	94.4	106.2	121.7	132.0	143.1
E_{lab}/A (MeV)	9.33	10.42	11.81	12.67	13.73
σ_{fus} (mb) [a]	1449	1512	1577	1609	1644
σ_{ER} (mb) [b]	1449	1496	1527	1537	1544
l_{crit}	50.1	54.0	58.9	61.6	64.9
l_{ER}	50.1	53.7	57.95	60.2	63.4
$\langle M\rangle_{\overline{xn}}$	18.7 7	21.6 9	20.85 35	21.3 8	21.4 7
$\langle x\rangle$	7.05	7.41	8.39	8.96	8.98
$\langle M\rangle_{\overline{\alpha xn}}$	20.2 24	22.0 15	19.1 4 [c]	19.9 4 [d]	19.5 5
$\langle M\rangle_{\overline{\alpha xn+2p(x+2)n}}$			19.5 7	20.5 5	19.8 6
$\langle x\rangle_\alpha$	5.55	6.03	7.96	8.06	8.41
$\langle M_s\rangle$	4.9	5.1	5.4	5.6	5.8
f_s (adopted)	0.37	0.39	0.42	0.43	0.44
$\langle J\rangle_{\overline{xn}}$	29.4 14	35.0 18	33.2 7	33.8 16	33.8 14
f_n (deduced)	0.36 20	0.34 23	0.65 8	0.71 18	0.94 16
fl	0.36	0.34	2.5	3.1	5.3
$\langle J\rangle_{\overline{\alpha xn}}$	32.4 40	35.8 23	29.6 8	31.0 8	30.0 10
f_α	<2.9	<0.2	5.8	5.9 8	3.9 10

[a] Prediction of the Bass model, Ref. 30.
[b] From σ_{fus} with an empirical estimate of fission subtracted, the latter from Ref. 31.
[c] From analysis of the yield curves and multiplicity curves of Figs. 7(c)–7(d) and 7(h)–7(j) as discussed in Sec. V of the text.
[d] From the coincidence results of Ref. 15.

fusion cross sections. The fraction of the compound nuclei that decay by fission was estimated by an empirical correlation of $\sigma_{fission}$ and σ_{fus} from Ref. 31 for the same ^{170}Yb compound system. The results for σ_{fus} and σ_{ER} are given in Table V for ^{20}Ne + ^{150}Nd and in Table VI for ^{12}C + ^{158}Gd. The corresponding angular momenta are shown in Fig. 9. It may be noted that for the lowest two bombarding energies, where the *pxn* and fission channels are probably unimportant, sums of the (^{12}C, *xn*) and (^{12}C, αxn) cross sections from Table III are within 15% of the σ_{ER} predictions; allowing for the lack of ground-state extrapolations of σ_J, this is excellent agreement.

The average angular momentum $\langle J\rangle_{\overline{xn}}$ of the *xn* entry states is dissipated by γ rays according to the generally accepted picture that the entry state decays first by several "statistical" transitions, after which the nucleus de-excited by transitions along the yrast line or in bands parallel to it. Thus we obtain the relation

$$\langle J\rangle_{\overline{xn}} = f_y[\langle M\rangle_{\overline{xn}} - \langle M_s\rangle] + f_s\langle M_s\rangle , \tag{3}$$

where $\langle M_s\rangle$ is the average number of statistical transitions, $\langle M\rangle_{\overline{xn}} - \langle M_s\rangle$ is the average number of yrast transitions (except when $J_g \neq 0$), and f_s and f_y are the angular momentum removed on the average by each type of transition.

Previous analyses[29] from (HI, *xn*) reactions at lower excitation energies indicate that a linear relationship exists between $\langle M\rangle_{\overline{xn}}$ and $\langle l_{ER}\rangle$. Figure 10 combines the present data with earlier results[16,17] for ^{170}Yb to test for such a relation. (The open square is from ^{4}He + ^{166}Er at 67.5 MeV.[17] Although pre-equilibrium effects were observed at this energy, they account for <10% of the total reaction cross section.) With the exception of the three points from the higher ^{12}C energies, the results exhibit a linear dependence

$$\langle M\rangle_{\overline{xn}} = \frac{1}{f_y}\langle l_{ER}\rangle + C , \tag{4}$$

where $f_y = 2.06 \pm 0.06$ and $C = 2.6 \pm 0.3$. Here the

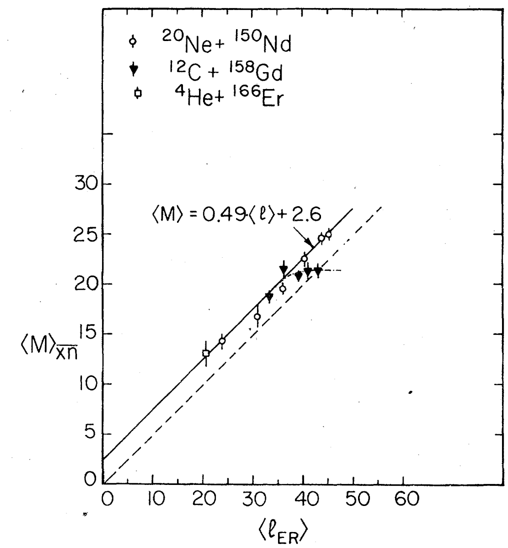

FIG. 10. Dependence of the total multiplicity $\langle M\rangle_{xn}$ for different systems at various bombarding energies on $\langle l_{ER}\rangle$, the average angular momentum of the initial compound states leading to the evaporation residues. The open circles and the square are from Refs. 16 and 17, while the full circles are from the present work. The solid straight line is a least-squares fit to the data, neglecting the three triangles from the higher energies of ^{12}C + ^{158}Gd. The dashed straight line is drawn through the origin with a slope of $\frac{1}{2}$.

identification of f_y as the coefficient of $\langle M\rangle_{\overline{xn}}$ from Eq. (3) has been adopted. The value of 2.6 ± 0.3 for C is consistent with $C = 4.0 \pm 0.3$ from Beene *et al.*[29] in view of the fact that they did not correct their $\langle M\rangle$ values for response of the NaI detectors to neutrons; our result without this correction would be similar to theirs. Combining all these results we obtain

$$f_n\langle x\rangle + f_s\langle M_s\rangle = f_y[\langle M_s\rangle - C] . \tag{5}$$

In the following analysis we take $f_y = 2$ and $C = 2.6$. A preliminary estimate of $\langle M_s\rangle$ from unfolded NaI spectra[32] from the ^{20}Ne + ^{150}Nd reactions at an excitation energy E^* of 80 and 115 MeV

TABLE VII. Possible values of the angular momentum f_n and f_s removed per neutron and per statistical γ ray consistent with the ^{150}Nd(^{20}Ne, *xn*) reactions at the indicated excitation energies.

E^* (MeV)	$\langle x\rangle$	$\langle M_s\rangle$	(a) $f_n\langle x\rangle = f_s\langle M_s\rangle$ f_s	f_n	(b) $f_n\langle x\rangle = 1.5f_s\langle M_s\rangle$ f_s	f_n	(c) $f_n\langle x\rangle = 2f_s\langle M_s\rangle$ f_s	f_n
63.2	5.09	4.3	0.40	0.34	0.32	0.40	0.26	0.44
77.7	6.06	4.6	0.43	0.33	0.35	0.40	0.29	0.45
93.7	6.9	4.8	0.46	0.32	0.37	0.38	0.31	0.43
107.0	7.5	5.1	0.49	0.33	0.39	0.40	0.33	0.44
124.3	8.6	5.5	0.53	0.34	0.42	0.40	0.35	0.45
132.0	9.0	5.6	0.54	0.34	0.43	0.40	0.36	0.44

gives $\langle M_s\rangle = 3.1 + 0.019E^*$ (E^* in MeV). This in turn provides a relation between f_s and f_n via Eq. (5). Table VII shows the possible values of f_s and f_n based on three assumptions: (a) $f_n\langle x\rangle = f_s\langle M_s\rangle$, (b) $f_n\langle x\rangle = 1.5f_s\langle M_s\rangle$, and (c) $f_n\langle x\rangle = 2.0f_s\langle M_s\rangle$. A simple statistical model calculation, assuming a J-dependent level density with a spin cut-off parameter corresponding to the rigid body moment of inertia, indicates that f_s is ~0, 0.5, or 0.9 for an initial J of 1, 20, or 40, respectively. For the same transition energy and large J, similar results are obtained for f_n. Since Table VII shows that assumption (b) gives $f_s \approx f_n$, this assumption was adopted for this work. In simplified treatments it is often assumed that on the average the statistical transitions remove no angular momentum ($f_s = 0$); this would require $f_n = 0.67$ for all the bombardment energies considered in this work.

The above analysis gives values for $\langle J\rangle_{\overline{xn}}$ via Eq. (3) consistent within experimental error with the results from Ref. 16.

We consider next the angular momentum balance following the (^{20}Ne, αxn) and (^{12}C, αxn) reactions. In this case Eq. (2) becomes

$$\langle l_{\rm ER}\rangle = \langle J\rangle_{\overline{\alpha xn}} + f_n\langle x\rangle + f_\alpha\,, \qquad (6)$$

where f_α is the average angular momentum removed by the α particle. Determination of $\langle M\rangle_{\alpha xn}$ for use in the analog of Eq. (3) is complicated by the presence of the $2p(x+2)n$ reactions. The saturation effects at small x may be different for αxn and $2p(x+2)n$, so it is not possible with the data of this experiment alone to extract the contribution due to the αxn channels. In the α-γ coincidence experiments at 152 MeV,[15] the αxn multiplicities were determined without $2p(x+2)n$ interference. On the basis of these results and curves of similar shape assumed for the 141.7- and 164.7-MeV data, estimates were made of $\langle M\rangle_{\alpha xn}$. The average values, $\langle M\rangle_{\overline{\alpha xn}}$, as well as the averages for the $2p(x+2)n$ products, are given in Table VI for all five ^{12}C bombardments. The deduced values of $\langle J\rangle_{\overline{\alpha xn}}$ and f_α are also listed. It should be pointed out that $\langle M\rangle_{\overline{\alpha xn}}$ need not vary linearly with $\langle l_{\rm ER}\rangle$ because of the presence of the f_α term in Eq. (6); for the ^{20}Ne + ^{150}Nd system f_α was found to vary with bombardment energy.[16] We shall return to the point of angular momentum removed by the α particles in Sec. V B.

Next, we relate the width σ_M of the measured multiplicity distribution describing all exit channels at each bombarding energy to $\langle l_{\rm ER}\rangle$. These widths can be obtained either by constructing the actual multiplicity distribution from the sum of those for the individual exit channels using the first three moments $\langle M\rangle_x$, σ_M, and s_M, or from $\langle M^2\rangle$ obtained as a weighted average of $\langle M^2\rangle = \sigma_{M_x}{}^2 + \langle M\rangle_x{}^2$ using cross sections for each exit channel as weights. The results of the latter analysis are shown in Fig. 11. An essentially linear dependence of σ_M is observed, which may be represented by $\sigma_M = 1.82 + 0.153\langle l_{\rm ER}\rangle$. The solid line in Fig. 11 gives for comparison the width of a triangular distribution ($\frac{1}{2}\sigma_l$) with average value $\langle l_{\rm ER}\rangle$. (The value of σ_l is $\langle l_{\rm ER}\rangle/\sqrt{8}$, and the factor $\frac{1}{2}$ accounts for the relation between multiplicity and angular momentum for yrast transitions.) Clearly σ_M is larger than $\frac{1}{2}\sigma_l$ by about 0.8–1.4 units. If all of this excess broadening is attributed to the statistical transitions, then their contribution σ_{M_s} is ~4.3. Here we have assumed that the yrast cascade makes no significant contribution to the width. However, comparison with a triangular entry-state population is probably unrealistic. The entry-state distribution results from an initial l distribution of the fused system which is rounded, not triangular, and is subject to broadening by the subsequent neutron emission. Both of these effects will make the entry-state distribution wider than a triangular one. By an analysis similar to that in Refs. 17 and 29, it can be shown that $\sigma_{M_s} \sim 3.2$ for these data. This is consistent with recent experiments on the multiplicity of the γ continuum from ^{20}Ne + ^{150}Nd at excitation energies near 90 MeV,[32] and is similar to the estimate $\sigma_{M_s} \sim 2.8$ made in Ref. 29.

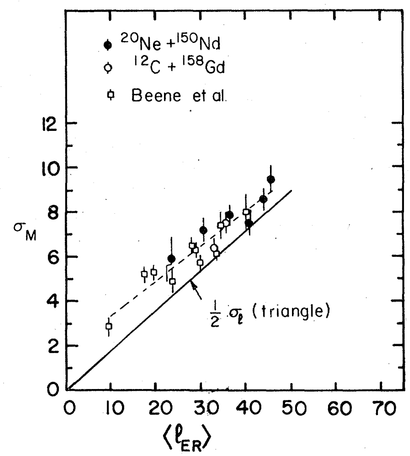

FIG. 11. Width σ_M of the overall multiplicity distribution for different systems at various energies, plotted as a function of $\langle l_{\rm ER}\rangle$. The full circles are from Refs. 16 and 17, the open squares from Ref. 29, and the open circles are from the present work. The dashed line is a least-squares fit to the data, while the full line shows what would be expected for a sharp-cutoff distribution of initial compound states with no allowance for broadening by the neutron emission and the statistical cascade.

We will defer discussion of the skewness until the end of the next section.

B. Angular momentum distributions in each exit channel

We turn our attention first to deducing the average angular momentum $\langle J\rangle_x$ for the entry states leading to each exit channel xn. Since the multiplicity $\langle M_J\rangle$ is independent of J (Fig. 4), we can assume that relations similar to Eq. (3) apply to each exit channel. If we assume further that f_y, f_s, and $\langle M_s\rangle$ are the same for all channels, we obtain

$$\langle J\rangle_x = J_g + f_y[\langle M\rangle_x - \langle M_s\rangle] + f_s\langle M_s\rangle \ . \qquad (7)$$

Note that the ground-state spin J_g is explicitly stated because $\langle M\rangle_x$ does not include it; J_g differs markedly for adjacent values of x. We take $f_y = 2$ and adopt the values of f_s and $\langle M_s\rangle$ given in Tables V and VI for the ^{20}Ne and ^{12}C reactions. For the three higher ^{12}C energies the values of f_n were deduced from Eq. (5) using case (b) of Table VII for f_s. These f_n values are considerably higher than those for the ^{20}Ne because of pre-equilibrium evaporation of neutrons.

We consider next the relation of the widths of the multiplicity distribution σ_{M_x} to the width σ_{J_x} of the J distribution for the entry states in each exit channel. In analogy with Eq. (5) of Ref. 17 we write, omitting the small cross term,

$$\sigma_{M_x}{}^2 = \frac{1}{f_y{}^2}\sigma_{J_x}{}^2 + \left(1 - \frac{f_s}{f_y}\right)^2 \sigma_{M_s}{}^2 \ . \qquad (8)$$

In the analysis of the ^{12}C + ^{158}Gd reactions at excitation energies of 94.4 and 121.7 MeV a value for $\sigma_{M_s}{}^2 \sim 10$, in accordance with the previous estimate, was used in Eq. (8) for each individual exit channel in order to obtain σ_{J_x} from the measured σ_{M_x} values.

Finally, we must relate the measured skewness s_{M_x} of the multiplicity distributions to s_{J_x}, the skewness of the entry-state distribution for each channel. The values for s_{M_x} (shown in Table IV) are subject to large statistical uncertainties, but are generally between 0 and -0.8. (A negative skewness means a tail on the low side of the distribution.) Decomposition of s_{M_x} into components due to the yrast and to the statistical part is not practical with the present data. In constructing J distributions in the entry states it has been customary either to ignore[17,33] the skewness (take $s_{M_x} = 0$), or to take it approximately equal[16] to s_{M_x}. In this work, the same skewness s_x was used for all channels, and the calculations were repeated with different choices of s_x to demonstrate its effect on the shape of the total spin distribution.

If all the moments are known, one may construct the distribution using an expression from Ref. 34. If the moments above the third are set to zero, this expression for the probability of spin J [or partial cross sections $\sigma(J)$ in this case] reduces to

$$\sigma(J) = \frac{A}{\sigma_0\sqrt{2\pi}} \exp\left[-\frac{(J-J_0)^2}{2\sigma_0{}^2}\right] \times\left\{1 + s_0\left[\frac{4}{3}\left(\frac{J-J_0}{\sigma_0}\right)^3 - 2\left(\frac{J-J_0}{\sigma_0}\right)\right]\right\}, \qquad (9)$$

where A is the area, J_0 the average value, σ_0 the standard deviation, and s_0 the skewness. The distributions for each exit channel were constructed by retaining only the positive part of Eq. (9). Since this modified distribution no longer has the same moments, the parameters of Eq. (9) were adjusted by iteration to reproduce the experimental values.

The calculated spin distributions for the xn channels from the ^{12}C + ^{158}Gd reactions at 112 MeV are shown in Figs. 12(a)–12(c) for three choices of s_x. The vertical arrows indicate the $\langle J\rangle_x$ values. It is seen that even though $\langle J\rangle_x$ moves down appreciably as x increases, the observed overlap extends over several exit channels. Interestingly, the skewness of the resulting sum distribution (labeled "total xn") is small ($s = -0.03$) for the symmetric case ($s_x = 0$), and is essentially independent of s_x for s_x of -0.33 and -0.48. In Fig. 12(d) the J distributions in the entry states from the (^{12}C, αxn) channels are shown. These were constructed assuming $s_x = -0.3$. Again a downward displacement in $\langle J\rangle_{\alpha xn}$ with x and a strong overlap are clearly seen. Figure 12(e) shows the the total xn and αxn distributions together with their sum.

The entry-state J distributions constructed for the 141.7-MeV experiment show some essentially different features traceable in part to the saturation in xn multiplicity mentioned earlier; only $\langle J\rangle_{10}$ is appreciably lower than the other $\langle J\rangle_x$ values (Fig. 6). Other major differences occur because the observed widths are larger and the measured skewness more negative. Thus the J distributions are very broad and have a large asymmetry toward the small J values. In Figs. 13(a) and 13(b) the xn J distributions calculated with $s_x = -0.23$ and -0.39 are shown. Again the vertical arrows in Fig. 13 indicate the values of $\langle J\rangle_x$ and the values in parentheses give the skewness of the sum distributions. These distributions have significant population at $J = 0$ as a consequence of the large widths and negative skewness. The experimental results in Table IV for the 141.7-MeV data favor even greater (more negative) skewness, but Eq. (9)

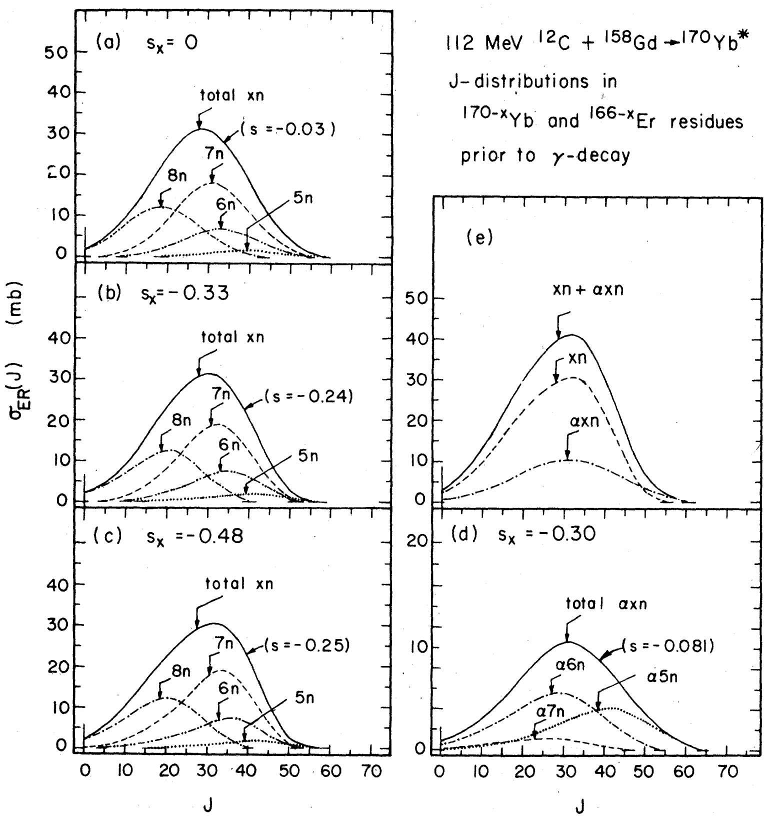

FIG. 12. Angular-momentum distributions in the entry states of the evaporation residues from the (^{12}C, xn) and (^{12}C, αxn) reactions at 112 MeV. The curves in (a), (b), and (c) were calculated with three values of the skewness in each exit channel, namely, $s_x = 0$, -0.33 and -0.48, respectively. The vertical arrows give $\langle J \rangle_x$ for each product. The values of s in parentheses give the skewness for the sum ("total xn") distribution. The curves in (d) give the J distributions in the (^{12}C, αxn) channels. The dashed and dash-dot curves in (e) give the total αxn (for $s_x = -0.48$) and xn distributions copied from (c) and (d) and the solid curve represents their sum.

then produces distributions with much larger values at $J = 0$. It is possible to incorporate more negative values of s_x and retain the same values for the first two moments by making the falloff at high J values steeper than that given by Eq. (9). An example of this is shown in Fig. 13(c) where $s_x = -0.56$. Figure 13(e) shows the three distributions from all the xn channels together for comparison. In Fig. 13(d) we show the distributions calculated with $s_x = -0.25$ for the channels leading to $^{166-x}Er$ products. These are principally due to αxn reactions and are so labeled. The distributions for all the xn and αxn channels and their sum are shown in Fig. 13(f). The αxn curve clearly gives more emphasis to the lower spin values than the 112-MeV results of Fig. 12(e).

The entry-state J distributions for the bombardments at 152.0 and 164.7 MeV are very similar to those for 141.7 MeV because the multiplicities and the widths at the higher energies are essentially the same as at 141.7 MeV.

V. DISCUSSION

A. Angular momentum removed by the first neutron

It was pointed out in Sec. III that the results from the multiplicities in the $^{12}C + {}^{158}Gd$ reactions, unlike those for $^{20}Ne + {}^{150}Nd$,[16,17] exhibit a remarkable deviation from the behavior that would be expected with compound nucleus formation and decay, similar to that observed for (^4He, xn) reactions[17] which are known[11] to involve pre-equilibrium neutron emission. It is instructive to estimate the average angular momentum f_1 removed by the first neutron. If we assume that it is the only pre-equilibrium particle emitted, we obtain

$$f_1 = \langle l_{ER} \rangle - \langle J \rangle_{xn} - f_n(\langle x \rangle - 1) \,, \tag{10}$$

where f_n is taken from the ^{20}Ne data of Table V for the same excitation energy. The values of $\langle J \rangle_{\overline{xn}}$ were derived from the smooth curve through the closed triangles in Fig. 9 in order to minimize scatter due to statistical errors. The results for f_1 are given in Table VI as a function of bombarding energy. At 112 and 125 MeV f_1 is no different from f_n (the average over all the neutrons). Above 125 MeV its value jumps suddenly by an order of magnitude, just where the multiplicity ceases to follow the increasing trend with input angular momentum (Fig. 10).

The values for f_1 are consistent with the emission of a fast neutron of reasonable energy and impact parameter. For example, at 152-MeV bombarding energy, $f_1 = 3.2$. The spectra in the following paper[15] indicate that the neutrons in the hard component correspond to a temperature

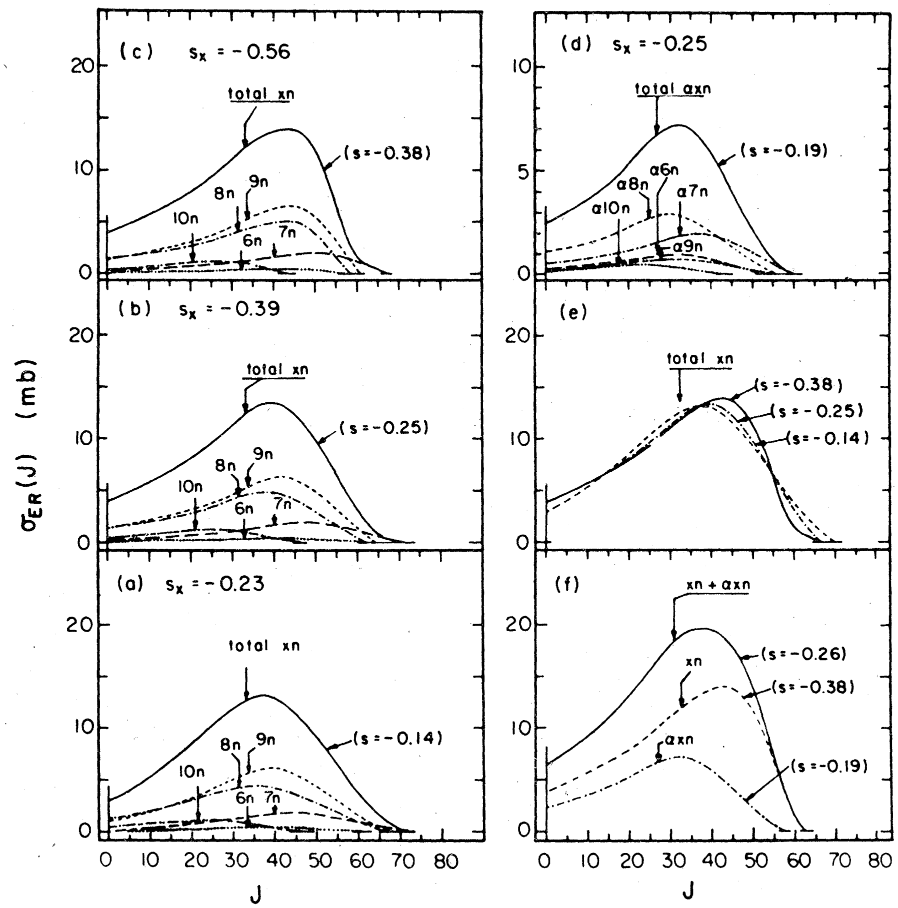

FIG. 13. The curves shown are derived from the 141.7-MeV $^{12}C+^{158}Gd$ data and have the same meaning as in Fig. 12. Note the extensive overlap of all channels, and the effect of different values of the skewness on the shape of the distributions. In (*f*) the total xn and αxn distribution is shown.

$t=6$ MeV and therefore have average energy $2t$ $=12$ MeV. A neutron of this energy would carry away $5.2\hbar$ if emitted at the grazing distance (less if emitted at a smaller distance).

The estimates of f_1 made thus far conceal a possible dependence on exit channel. This might be expected because the channels involving the largest number x of emitted neutrons probably involve only equilibrium reactions. We can make a rough estimate of the x dependence of f_1. The dash-dot line in Fig. 6(i), based on systematic extrapolation from the data in Figs. 6(f)-6(h), indicates what might be expected if pre-equilibrium effects were absent. The measured $\langle M\rangle_8$ is about three units below this line, which implies that on the average six units of angular momentum are removed by pre-equilibrium emission. If only one fast neutron of average energy were involved, then as discussed above it would be possible for it to remove a maximum of $5.2\hbar$. It thus seems likely that emission of more than one pre-equilibrium neutron occurs in the decay leading to the $8n$ product. Similarly, processes leading to the $7n$ or $9n$ products probably include a larger or smaller number of pre-equilibrium neutrons, respectively.

B. Angular momentum removed by α particles

The angular momentum balance in the ($^{20}Ne, \alpha xn$) reactions has been reanalyzed by applying Eq. (6) to the data from Ref. 16 and a point at lower energy from Ref. 17. The deduced f_α values are given in Table V. Within experimental error they are in agreement with the results of the somewhat different analysis given in Ref. 16 (there labeled $\bar{l}_\alpha$). For the higher bombardment energies about $10\hbar$ are required for the balance of angular momentum. Either this much angular momentum is removed on the average by the α particle or else the αxn channels must originate primarily from the lower J part of the initial population. The latter explanation is doubtful because the systematic downward displacement of the J distribution in the αxn channels as x increases (Figs. 8 and 9 of Ref. 16) suggests that all angular momenta are involved in these reactions.

In the $^{12}C+^{148}Gd$ reactions at the three highest energies the $^{166-x}Er$ products are produced either by αxn or by $2p(x+2)n$ evaporation (Fig. 7), while in the $^{20}Ne+^{150}Nd$ reactions[16,17] only the αxn processes appear to be present. However, the coincidence experiments[15] show that the *fraction* of $2p$ emission for $^{20}Ne+^{150}Nd$ is quite substantial at 132 MeV excitation, about half that for $^{12}C+^{158}Gd$ (Table III of Ref. 15). Much more energy is required for $2p(x+2)n$ evaporation than for αxn decay, so that one expects the former products to originate primarily from a lower-J region of the initial distribution where the available thermal energy is larger. This is borne out by the observation [Figs. 7(h)–7(j)] that the γ-ray multiplicity for the $2p(x+2)n$ channels in $^{12}C+^{158}Gd$ is below that of the αxn channels for the same x. The same effect is seen clearly in the $^{20}Ne+^{150}Nd$ coincidence results (Fig. 3 of Ref. 15). The fact that the $2p$ fraction is stronger in the ^{12}C reactions can also be explained. The population of the lower-J compound states that give rise to $2p$ emission is proportional to $\pi \lambda^2$, which is 1.7 times larger for $^{12}C+^{158}Gd$ than for $^{20}Ne+^{150}Nd$ at the energies of Ref. 15.

The question of pre-equilibrium emission of α particles should also be discussed. As was pointed out earlier, the values of $\langle M\rangle_{\alpha xn}$ vs x [Figs. 7(h)–7(j)] suggest a saturation at low x values. The $\langle M\rangle_{\alpha xn}$ values calculated in Sec. IV A and the deduced $\langle J\rangle_{\alpha xn}$ given in Table VI were used to derive the values of J_{max} plotted in Fig. 14 as the full circles. Here J_{max} is the minimum angular momentum in the entry states. The open circles are the J_{max} values for the ($^{20}Ne, \alpha xn$) reactions, derived from the $\langle J\rangle_{\alpha xn}$ of Table V. The dash-dot and solid curves are the l_{ER} values (maximum angular momentum of the initial states that lead to evaporation) for $^{12}C+^{158}Gd$ and $^{20}Ne+^{150}Nd$ from Fig. 9. For the ^{20}Ne case, as the excitation energy increases, J_{max} increases at a much lower rate than does l_{ER}, indicating that increasingly larger amounts of angular momentum are being removed by the α particles. For ^{12}C, J_{max} first appears to increase and then drastically decreases. This suggests the onset of a different mechanism for the removal of the angular momentum by the α particles, perhaps a pre-equilibrium evaporation.

It is interesting to correlate the average angular momentum f_α removed by the α particle with the input angular momentum l_{ER} from both the ^{20}Ne and ^{12}C experiments. This is shown in Fig. 15, a plot of data given in Tables V and VI. A rapid increase in f_α is observed when $l_{ER} \gtrsim 50$. The data suggest that the angular momentum l_α removed by

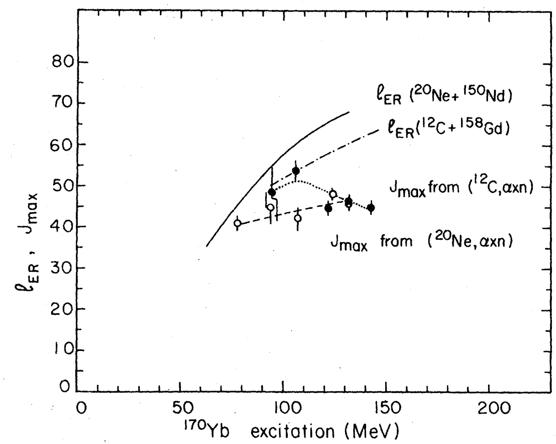

FIG. 14. Variation of maximum angular momenta for $^{166-x}Er$ products prior to γ decay, as a function of excitation energy. The solid line gives the l_{ER} values for $^{20}Ne+^{150}Nd$. The open circles give the $J_{max,\overline{\alpha xn}}$ values from γ-ray multiplicity measurements. The dash-dot curve gives the l_{ER} values for $^{12}C+^{158}Gd$ and the full circles the $J_{max,\overline{\alpha xn}}$ values from γ-ray multiplicity measurements. The dashed and dotted lines drawn through the data points are to guide the eye.

the α particles emitted from the high-l initial states is much more than for the low-l states. Furthermore, since f_α is large at high excitation, a wide range of l_α values is possible. This can produce broad J distributions in the entry states even if the initial α-emitting states are confined to a narrow band at high l. The calculated αxn J distributions are, in fact, broader at high energy than at low [compare Figs. 12(e) and 13(f) for ^{12}C, and Figs. 8(c) and 9(c) of Ref. 16 for ^{20}Ne].

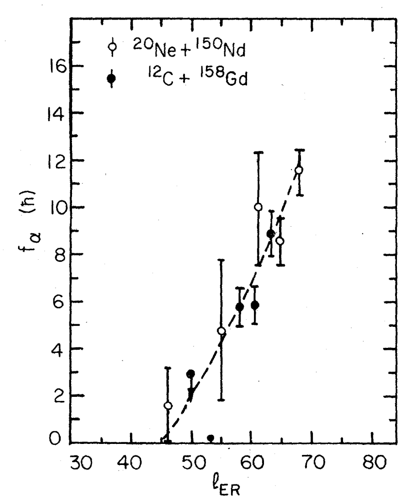

FIG. 15. The full and open circles give the deduced average angular momentum f_α removed by the α particle in αxn reactions for $^{20}Ne+^{150}Nd$ and $^{12}C+^{158}Gd$, respectively, as a function of the maximum input angular momentum l_{ER}.

C. Summary

The saturation effects observed in the γ-ray multiplicity are a clear indication of pre-equilibrium emission of neutrons in the $^{12}C+{}^{158}Gd$ reactions. These do not appear in earlier data on $^{20}Ne+{}^{150}Nd$ at the same compound-nucleus excitation energy. They seem to set in at a bombardment energy ≥ 10 MeV per nucleon. The angular momentum removed by the pre-equilibrium neutrons increases sharply at and above a bombarding energy of 141.7 MeV. The angular-momentum distributions of the entry states, inferred from the measured moments of the multiplicity distribution, change markedly at this energy, becoming broader and favoring more strongly the entry states of low angular momentum. Some indication of pre-equilibrium α emission was found from multiplicity measurements for the αxn channels. Much of the $^{166-x}Er$ produced is the result of $2p(x+2)n$ emission.

ACKNOWLEDGMENTS

The excellent cooperation of the staffs of the Oak Ridge Isochronous Cyclotron and of the Washington University cyclotron is appreciated. We are grateful to Mr. J T. Hood and to the crew of the Washington University cyclotron machine shop for the design and construction of the apparatus. We thank S. Gronemeyer for assistance in collection of part of the data. Those of us visiting at ORNL (D.G.S., L.W., and J.H.B.) wish to acknowledge the hospitality extended to us during our stay. One of us (D.G.S.) acknowledges a summer faculty participation fellowship from Oak Ridge Associate Universities. This work was supported in part by the U.S. Department of Energy under Contract No. EY-76-S-02-4052. Oak Ridge National Laboratory is operated by Union Carbide Corporation for the U.S. Department of Energy, Division of Basic Energy Sciences, under Contract No. W-7405-eng-26.

*Present address: Institute of Physics, University of Uppsala, Uppsala, Sweden.

[1]A. Fleury and J. M. Alexander, Ann. Rev. Mod. Phys. 24, 279 (1974), and references therein.

[2]R. G. Stokstad, in Proceedings of the Fall Creek Falls Meeting on Heavy-Ion Collisions, Pikeville, TN., June 13–17, 1977 (unpublished), [CONF-770602, and references therein.

[3]J. Gilat, E. R. Jones, III, and J. M. Alexander, Phys. Rev. C 7, 1973 (1973).

[4]J. M. Alexander and G. N. Simonoff, Phys. Rev. B133, 93 (1974).

[5]H. Gauvin, Y. LeBeyec, M. Lefort, and R. L. Hahn, Phys. Rev. C 10, 722 (1974).

[6]Y. LeBeyec, R. L. Hahn, K. S. Toth, and R. Eppley, Phys. Rev. C 14, 1038 (1976).

[7]R. G. Stokstad, J. Gomez del Campo, J. A. Biggerstaff, A. H. Snell, and P. H. Stelson, Phys. Rev. Lett. 36, 1529 (1976).

[8]F. P. Pühlhofer, Nucl. Phys. A280, 267 (1977).

[9]H. C. Britt, B. H. Erkkila, P. D. Goldstone, R. H. Stokes, F. Plasil, R. L. Ferguson, and H. H. Gutbrod, in Proceedings of the Symposium on Macroscopic Features of Heavy-Ion Collisions, Argonne, 1976 [ANL/PHY-76-2 (unpublished)], p. 491.

[10]F. Plasil, paper presented at the Winter Meeting on Nuclear Physics, Bormio, Italy, January 17–21, 1977 (unpublished).

[11]M. Blann, Nucl. Phys. A235, 211 (1974).

[12]J. Galin, B. Gatty, D. Guerreau, C. Rousset, U. C. Schlotthauer-Voos, and X. Tarrago, Phys. Rev. C 9, 1126 (1974).

[13]T. Nomura, H. Utsunomiya, T. Motobayashi, T. Inamura, and M. Yanokura, Phys. Rev. Lett. 40, 694 (1978).

[14]N.-H. Lu, D. Logan, J. M. Miller, T. W. Debiak, and L. Kowalski, Phys. Rev. C 13, 1496 (1976).

[15]L. Westerberg, D. G. Sarantites, D. C. Hensley, R. A. Dayras, M. L. Halbert, and J. H. Barker, following paper, Phys. Rev. C 18, 796 (1978).

[16]D. G. Sarantities, J. H. Barker, M. L. Halbert, D. C. Hensley, R. A. Dayras, E. Eichler, N. R. Johnson, and S. A. Gronemeyer, Phys. Rev. C 14, 2138 (1976).

[17]D. G. Sarantities, L. Westerberg, R. A. Dayras, M. L. Halbert, D. C. Hensley, and J. H. Barker, Phys. Rev. C 17, 601 (1978).

[18]M. L. Halbert, R. A. Dayras, R. L. Ferguson, F. Plasil, and D. G. Sarantites, Phys. Rev. C 17, 155 (1978).

[19]L. Westerberg, D. G. Sarantites, R. Lovett, J. T. Hood, J. H. Barker, C. M. Currie, and N. Mullani, Nucl. Instrum. Methods 145, 295 (1977).

[20]L. L. Riedinger, D. C. Hensley, P. H. Stelson, N. R. Johnson, G. B. Hagemann, R. L. Robinson, E. Eichler, R. O. Sayer, and G. J. Smith, Oak Ridge National Laboratory Report No. ORNL-4937, 1973 (unpublished).

[21]P.O. Tjøm, F. S. Stephens, R. M. Diamond, J. de Boer, and W. E. Meyerhof, Phys. Rev. Lett. 33, 593 (1974).

[22]W. Trautmann, D. Proetel, O. Häusser, W. Hering, and F. Riess, Phys. Rev. Lett. 35, 1694 (1975).

[23]A. Buyrn, Nucl. Data 11, 327 (1974); 17, 97 (1976).

[24]J. K. Tuli, Nucl. Data 9, 273 (1973); 12, 245, 477 (1974); 13, 493 (1974).

[25]T. W. Burrows, Nucl. Data 18, 553 (1976).

[26]H. Buescher, W. F. Davidson, R. M. Lieder, and C. Mayer-Böricke, Annual Report KFA Jülich, 1973 (unpublished).

[27]H. Buescher, W F. Davidson, R. M. Lieder, A. Neskakis, and C. Mayer-Böricke, Annual Report KFA Jülich, 1973 (unpublished).

[28]See AIP document No. PAPS PRVCA 18-774-18 for 18 pages of data on level cross sections, average multiplicities, and widths of the multiplicity distribution of the γ cascades in the reaction products from $^{12}C+{}^{158}Gd$. Order by PAPS number and journal refer-

ence from American Institute of Physics, Physics Auxiliary Publications Service, 335 East 45th Street, New York, New York 10017. The price is \$1.50 for microfiche or \$5 for photocopies. Airmail additional. Make checks payable to the American Institute of Physics. This material also appears in *Current Physics Microfilm*, the monthly microfilm edition of the complete set of journals published by AIP, on frames immediately following this journal article.

[29]J. R. Beene, O. Häusser, A. J. Ferguson, H. R. Andrews, M. A. Lone, B. Herskind and C. Bourde (to be published and private communication).

[30]R. Bass, Phys. Lett. 47B, 139 (1973); Nucl. Phys. A231, 45 (1974).

[31]A. M. Zebelman, L. Kowalski, J. Miller, K. Beg, Y. Eyal, G. Jaffe, A. Kandil and D. Logan, Phys. Rev. C 10, 200 (1974).

[32]L. Westerberg, D. G. Sarantites, K. Geoffroy, R. A. Dayras, J. Beene, M. L. Halbert, and D. C. Hensley, Bull. A. P. S. 23, No. 4 (1978).

[33]G. B. Hagemann, R. Broda, B. Herskind, M. Ishihara, S. Ogaza, and H. Ryde, Nucl. Phys. A245, 166 (1975).

[34]H. Margenau and G. M. Murphy, *The Mathematics of Physics and Chemistry*, (Van Nostrand, New York, 1943), p. 421.